Gulf General Atomic
Incorporated
P.O. Box 608, San Diego, California 92112

AEC RESEARCH AND
DEVELOPMENT REPORT

GA-9359

GAS-COOLED FAST BREEDER REACTOR

QUARTERLY PROGRESS REPORT
FOR THE PERIOD FEBRUARY 1, 1969 THROUGH APRIL 30, 1969

by

Project Staff

Prepared under
Contract AT(04-3)-167
Project Agreement No. 23
for the
San Francisco Operations Office
U.S. Atomic Energy Commission

Gulf General Atomic Project 393

June 12, 1969

CONTENTS

FIGURES

TABLES

1. INTRODUCTION

Gulf General Atomic Incorporated is in its sixth year of evaluating the Gas-Cooled Fast Breeder Reactor (GCFR) concept under Atomic Energy Commission (AEC) sponsorship. The program effort consists of four tasks: program planning, core development, testing, and reactor physics.

The broad objectives of the four tasks and the current efforts on each task are summarized below.

1.1. TASK A — PROGRAM PLANNING

The objective of this task is to prepare a plan for development and demonstration of the GCFR concept. This plan is based on privately sponsored plant design studies for purposes of defining the proposed GCFR operating environment.

The planning effort continued to be focused on the preparation of a detailed plan defining the work required to develop a proven core design. A revision to portions of the Core Development Plan, modified to include the necessary evaluation of the metal swelling phenomenon that occurs in a fast-flux environment, was submitted to the AEC. Further updating of the Core Development Plan will be made upon reviewing comments from the AEC and Oak Ridge National Laboratory reviewers.

1.2. TASK B — CORE DEVELOPMENT

The objectives of this task are (1) the review of work from related programs that is applicable to the GCFR, particularly work related to the Liquid-Metal Fast Breeder Reactor (LMFBR), (2) further detailed analysis of the reference fuel-rod concept, and (3) analysis of engineering details of alternative core design concepts.

The potential application of vanadium-based alloys as backup cladding material in fast-reactor designs was examined during this period. These alloys have excellent neutronic characteristics, greater high-temperature strength compared to that of stainless steels, and apparently better resistance to neutron irradiation damage at temperatures of interest for the LMFBR. For the GCFR, the gas coolant and the higher operating temperature are the primary factors in considering vanadium alloys as cladding material. The most severe problem would be contamination of the cladding by impurities in the gas stream. Furthermore, based on preliminary data, neither the high-temperature strength of vanadium nor its resistance to radiation may be adequate above 800°C.

The manifolded fuel rod has been selected as the reference concept for further analysis, which results in a high degree of similarity with the LMFBR fuel-rod designs. The current efforts on analytical models to predict the in-pile performance of fuel rods will be applicable to both GCFR and LMFBR design conditions.

The fuel-cladding-interacting fuel rod utilizing a relatively heavy cladding was selected as the alternative fuel-rod design. The current effort included a review of the methods being used to study the deformation and creep collapse of the cladding as a result of the external pressure differential.

Analytical models developed to predict the in-pile performance of fuel rods include the CRECOL, BRASH, and BRITL computer programs. The CRECOL code was developed for predicting creep-collapse characteristics of initially out-of-round cladding under external pressure during reactor operating conditions. The creep of cladding occurs as a function of time, stress level, and temperature. The strain-stress deformation resulting in cladding ovality and creep collapse is calculated by timesteps. Several options in the code permit the reactor designer to appraise the effects of several variables in order to produce a design with an adequate margin of safety. BRASH was used to investigate fuel-cladding interactions over the GCFR fuel-rod lifetime, but treated the fuel pellet as a continuous body, and cracks due to high thermal stresses were not taken into account. BRITL, which accounts for radial cracks in the fuel pellets, calculates the radial temperature distribution and thermal conductivity. It has been used to interpret the applicability of fast-reactor fuel-rod irradiation data obtained in a thermal reactor.

1.3. TASK C — TEST PROGRAM (IN-PILE AND OUT-OF-PILE TESTS)

The in-pile and out-of-pile tests are part of the overall fuel-element development program for the GCFR. Fuel irradiation in the Oak Ridge Research Reactor (ORR) is part of a joint GGA-ORNL program in the screening tests of fuel-rod materials and the selection of a fuel-rod concept. Irradiations in thermal-flux and fast-flux environments are to be conducted in the GCFR fuel-development program. Out-of-pile testing includes thermal cycling a section of a fuel rod under simulated GCFR pressure and temperature conditions to study fuel-cladding interaction.

Postirradiation examination of capsule 04-P8 is still in progress. The capsule, which contained three sealed-can, fuel-cladding-interacting fuel-rod specimens fueled with 12 wt-% PuO_2—88 wt-% UO_2 enriched to 9% U^{235}, was irradiated to exposures ranging from 47,000 to 59,000 MWD/tonne at linear heat ratings from 13.2 to 15.5 kW/ft and cladding OD temperatures from 610° to 685°C. A comparison of dimensional measurements before and after irradiation showed little or no change. The fission-product gases are being identified and analyzed. Further postirradiation examination will include burnup analysis, metallographic examination, and mechanical-property tests.

The planned irradiation program includes completion of the fabrication of a manifolded fuel-rod specimen for the capsule 04-P9 thermal-flux (ORR) test and the design of the subassembly (F-1) for fast-flux testing in EBR-II.

Capsule 04-P9 will contain one fuel-rod specimen, GA-20, that is designed to study the manifolded fuel-rod concept. The rod will be irradiated to a burnup of >50,000 MWD/tonne at a linear heat generation rate of 15 kW/ft. The fuel rod will have a maximum outer surface temperature of 700°C, and the fission-product trap will operate at an outer surface temperature of ∿300°C. This test is designed to yield information on fission-product release, fission-product distribution in the trap, fission-product trapping efficiency, fuel swelling, and fuel-cladding mechanical and chemical interactions.

The design of the capsules for fast-flux irradiation testing in an EBR-II subassembly is continuing. Each capsule will contain one plutonium-uranium-oxide fueled rod clad in 316 stainless steel, which will simulate a manifolded rod operating at nominal GCFR demonstration plant conditions: an average burnup of ∿50,000 MWD/tonne, heat generation rates of ∿15 kW/ft, and a maximum cladding temperature of 650° to 750°C.

In laboratory experiments to determine the release of noble gases from the GCFR fuel element, measurements of the diffusion coefficient for the gas pairs krypton-helium and xenon-helium and the absorption coefficient for krypton and xenon on activated carbon are being continued. These data are input to computer calculations for estimating fission-product-release fractions from the manifolded fuel rods. The SLIDER program is used for the analytical studies. Results of the analysis of the krypton diffusion experiments are in close agreement with experiments.

Improved test chambers for out-of-pile testing have been installed on the thermal-cycling rig, and checkout test runs have been made at 8, 10, and 12 kW/ft. The first 8 kW/ft test was unsuccessful due to thermocouple attachment problems. The second 8 kW/ft test ran for 258.1 hr with cladding temperatures from 780° to 880°C at 8.3 kW/ft and at 710° to 900°C at 7.1 kW/ft toward the end of the run. Tungsten vaporization from the center of the heater caused the drop in power. The 10 kW/ft test ran for 103.4 hr with cladding temperatures of 602° to 625°C. Metallographic examination of a transverse sample taken from near the midlength of the heated zone showed extensive grain growth in the UO_2 and that it was cracked radially, indicating a very high temperature at the surface of the central hole near the tungsten heater. Grain growth typical of UO_2 operation above 1800°C had occurred in this region and, although rapidly decreasing in extent, extended to the midradius of the fuel, indicating temperatures of 1500° to 1600°C in that area. The outer area of the UO_2 showed little change in structure. In the 12 kW/ft test, burnout occurred after 4 hr. Two more steady-state runs will be made at 12 and 14 kW/ft before cyclic testing is started.

1.4. TASK D — REACTOR PHYSICS PROGRAM

This task is directed toward a continuation of the critical experiments to be performed cooperatively with the Battelle Northwest Laboratory (BNWL) critical facility.

The program of critical experiments using plutonium fuel with an H:Pu ratio of 1:1 was started at Battelle Northwest. However, the amount of plutonium fuel in a 1:1 H:Pu ratio is not sufficient to construct a bare critical assembly. Therefore, a 5:1 ratio of H:Pu is being used as a driver in the 1:1 assemblies to achieve criticality; this is not expected to cause difficulties in the analysis of the 1:1 assemblies.

2. TASK A — PROGRAM PLANNING

In any large and complex engineering effort involving the development and application of new technology, it is essential that the major problem areas be identified early in the program, the functional requirements of systems and their interfaces be defined, and a comprehensive and systematic plan for accomplishing the desired goal be established. The purpose of Task A is to prepare plans for the development and demonstration of the Gas-Cooled Fast Reactor concept. The specific objectives are:

1. To coordinate overall criteria and requirements
2. To provide for general planning of tasks
3. To determine task priorities
4. To monitor programs and expenditures in relation to goals established
5. To update planning documents periodically as new technical information becomes available

As presently conceived, the working document outlining the program plan will consist of the following sections:

Section	Description
1000	Program Planning, Management and Projects
2000	Reactor Systems
3000	Reactor Auxiliaries
4000	Core Development
5000	Recycle Development
6000	Nonnuclear Systems
7000	Safety

Work on the document was initiated late in FY 67, with emphasis on preparation of the Core Development section. Funding limitations necessitate that completion of the working document be extended into FY 72.

A draft core development plan has been submitted to the AEC and updated to include the necessary evaluation of the metal-swelling phenomenon that occurs in a fast-flux environment. The Core Development section is the most critical portion of the overall plan in establishing the schedule for development and demonstration of the GCFR concept. The required fuel-irradiation program is the controlling item.

Comments from AEC and ORNL reviewers will be incorporated into the next updating of the core development plan. An outline of the Reactor Systems section will be prepared as the next activity.

3. TASK B — CORE DEVELOPMENT

3.1. CLADDING AND STRUCTURAL MATERIALS

The potential application of vanadium-based alloys in currently proposed and advanced designs has been examined. Owing to their desirable neutronic characteristics, their greater high-temperature strength relative to that of stainless steels, and their apparently better resistance to neutron irradiation at temperatures of interest for the LMFBR, vanadium alloys have received considerable attention as a backup cladding material. While this application appears technically sound with respect to the LMFBR, the oxygen content of the sodium coolant would have to be kept below 10 ppm to prevent catastrophic oxidation. This requirement can be met only by hot-trapping, which may or may not be feasible for a large reactor system but in any case allows very little leeway for any type of inleakage problem.

Two significant differences in the GCFR, the gas coolant and the higher temperature, require careful attention in considering vanadium as a useful cladding material for this type of reactor. The most severe problem is contamination of the cladding by impurities contained in the gas stream. Because of the high coolant pressure, the restrictions are even more stringent, since very small impurity contents, as measured at 1 atm, can be rapidly increased to significant partial pressures at the high total pressure employed. Despite an adequate purification system, any inleakage problem between the heat exchanger and the coolant stream would require complete cleanup even if reactor shutdown took place immediately. Based on very preliminary data, neither the high-temperature strength nor the irradiation resistance of vanadium appears adequate above about 800°C.

The basic problem thus consists of determining whether vanadium alloys can survive in a gaseous coolant, including consideration of accidents allowing inleakage of contaminants. Secondarily, more information must be generated relative to the irradiation stability of proposed alloys in the temperature ranges of interest for the gas-cooled reactor. Since vanadium alloys could be considered only for temperature ranges below about 800°C, perhaps before the extensive development work prerequisite to its use is initiated, surveys should be made of other alloy systems which might provide the capabilities for more severe operating conditions. Potential candidates are chromium-, molybdenum-, niobium-, and tungsten-based alloys.

3.1.1. Neutronics

Okrent (Ref. 1) has indicated that vanadium is among the most desirable metals from the standpoint of reactor physics. It is slightly superior to ferrous alloys and chromium, and significantly better than the other refractory metals.

3.1.2. Strength

Vanadium alloys have a clear-cut high-temperature-strength superiority over austenitic stainless steels (see Fig. 3.1)(Ref. 2). Both higher-strength nickel alloys and cobalt alloys have equivalent strengths, and other refractory metals are significantly stronger in the higher-temperature range. With reference to Fig. 3.1, the temperature at which each of these classes of metals would have a stress for 1% strain equivalent for 10,000 hr to austenitic stainless steel at 700°C is as follows:

	Temperature for Equivalent Resistance to Strain
Austenitic stainless steel.	700°C
Vanadium alloys, nickel-base alloys, and cobalt alloys.	810°C
Other refractory alloys	>1000°C

It appears that for strength considerations, vanadium alloys would be superior to the austenitic stainless steels and equivalent to commercially available nickel-base alloys for the GCFR commercial plant requirements.

3.1.3. Resistance to Coolant Contamination

No data are available on the corrosion of vanadium or vanadium alloys in a simulated GCFR environment. However, a picture of what behavior might be anticipated can be obtained by referring to sodium corrosion experience, contamination of niobium alloys *in vacuo*, and some data on gaseous interaction with vanadium.

In sodium corrosion, the phenomenology can be described as falling into three general categories:

1. A low rate of contaminant arrival at the metal surface. No surface layer is formed, and the rate of contaminant pickup is determined by the sticking coefficient and the diffusion of the contaminant away from the surface and into the bulk material. Although a surface layer of a second phase is not formed, there is commonly a hardening of the region into which the contaminant has diffused.

2. A medium rate of contaminant arrival at the metal surface. A surface film is formed which is continuous and somewhat protective. The rate of contamination of the metal is governed by the diffusion of the contaminant through the surface layer and commonly follows a parabolic relationship with time.

3. A high rate of contaminant arrival at the metal surface. A thick film is formed which may not be continuous or protective. It tends to flake off by errosion in a flowing system or as a result of thermal stresses during cycling. Generally, the rate of contamination is linear with time.

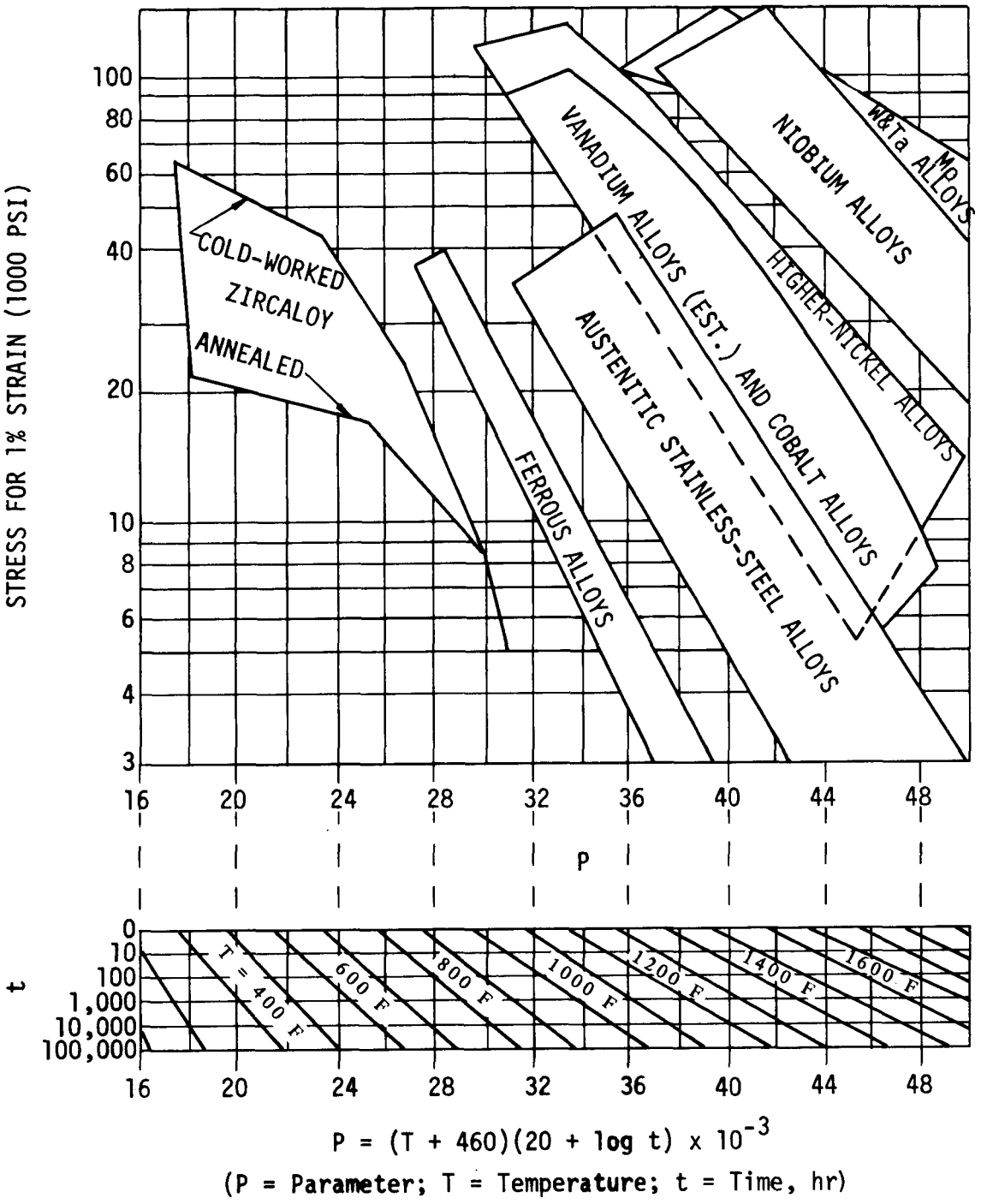

Fig. 3.1. Larson-Miller comparison of alloy systems, showing stress required to produce 1% strain (from Ref. 2)

The results of various sodium-corrosion experiments are given in Refs. 3 through 6, and the ranges of oxygen concentrations in the sodium which correspond to each of the above three types of phenomenology can be established from these results. Below about 5 ppm oxygen in the sodium, the first type of behavior is observed; in the range of 5 to 10 ppm oxygen in the sodium, the second type of behavior is found; and above 10 ppm oxygen, the last type of behavior is observed. At 20 to 28 ppm oxygen, only tens of hours elapsed before specimens lost one-half their initial weight in a flowing sodium system.

Alloying additions have been studied to improve the corrosion behavior of vanadium. Silicon, niobium, and chromium have been the most favorable alloying additions found to date, but in no case was an improvement in corrosion rate greater than a factor of three observed. Also, considerable core hardening has been observed in these alloys, indicating significant internal oxidation.

In conclusion, V-20 wt-% Ti, V-15 wt-% Ti—7.5 wt-% Cr, and V-5 wt-% Cr appear satisfactory for use in flowing sodium at 650°C if the oxygen level is kept below 10 ppm. No practical alloys have yet been found which permit operation at oxygen contents greater than 10 ppm. These restrictions place severe limitations on the use of vanadium alloys, but in well-controlled, hot-trapped systems they are perhaps usable. The problem may be less formidable in large reactor systems, where the volume of metal is large compared with the surface area from which contamination and inleakage can originate.

One useful piece of information derived from the sodium-corrosion data is that niobium is slightly more reactive than vanadium in a sodium environment. This observation substantiated some earlier work (Ref. 7) in which the reaction of pure vanadium with moderate oxygen pressures was studied in a gas system. Substantial oxidation rates were observed; however, vanadium was found to be somewhat more oxidation-resistant than niobium. This relationship can be used in conjunction with information obtained by Inouye and Roche in studies of the contamination of refractory metals by residual gases in hard vacuums. Inouye (Ref. 8) covered the range 600° to 1200°C at pressures between 10^{-6} and 10^{-8} torr and concluded that the maximum permissible pressure for long-time exposure of thin metal sections was in the range of 10^{-9} torr. This low level of contaminant, which is permissible, has been verified by Roche's investigations (Ref. 9) and other high-temperature creep work in which it has been determined that pressures of 10^{-8} to 10^{-9} torr are required to prevent alteration of mechanical properties by contamination. A relationship was established to describe the contamination of Nb—1 wt-% Zr alloys in the temperature range 750° to 1000°C:

$$\Delta c = \frac{90.6\ t(P)^{1/2} \exp - (5500/RT)}{X} ,$$

where Δc = increase in oxygen concentration due to contamination from one side (ppm),

t = exposure time (in hr),

P = system pressure (in torr),

X = specimen thickness (in in.).

If it is assumed that 1 ppm oxygen in a gas coolant is equivalent to $\sim 10^{-3}$ torr (i.e., if the interactions of the other gases present are ignored), then the above relationship can be used to describe the contamination of Nb–1 wt-% Zr under the following conditions: t = 30,000 hr, $P = 10^{-3}$ torr, T = 750°C, X = 0.015 in. It must be recognized that this is a very simplistic calculation which does not take into account a change in mechanism due to saturation of the metal with the contaminant. However, based on this calculation, $\Delta c = 3.6 \times 10^8$ ppm. Since a change of only 100 ppm would cause significant changes in mechanical properties, it can readily be seen that the system is unstable even at an impurity level of only 1 ppm. Under the EBOR development program at GGA, niobium alloys were tested in helium containing 10 ppm O_2 and 100 O_2, and the results were catastrophic.

In conclusion, contamination by impurities in the cooling gas appears to be the most severe problem associated with the use of vanadium alloys for gas-cooled reactors. This conclusion can be drawn for steady-state conditions even without referring to the problems associated with an accident allowing gross inleakage of air or water, or to the problems associated with protecting the system from contamination during the refueling cycle, which is performed at a moderate ($\sim$500°C) temperature level. If this class of alloys is to be considered, compatibility studies with impurities in the helium must be initiated early in the program.

3.1.4. Resistance to Irradiation Damage

A major problem associated with fast-reactor fuel cladding is the swelling and embrittlement observed in face-centered-cubic metals and alloys (such as austenitic stainless steel) after exposures to fast-neutron fluences considerably less than the $\sim 3 \times 10^{23}$ n/cm^2 expected during reactor operation. However, this phenomenon is noted only when the irradiation temperatures approach or exceed one-half of the absolute melting point, Tm/2. Because it has a higher melting point (Tm/2 $\sim$ 800°C) and owing to its body-centered-cubic structure, vanadium has been expected to prove more resistant to fast-neutron irradiation damage than stainless-steel or nickel-based-alloy systems. Preliminary irradiation results (Refs. 10-16) have supported this premise. Pure vanadium does appear susceptible to embrittlement, but titanium-containing vanadium alloys have been irradiated to a fast-neutron fluence of 3×10^{22} n/cm^2 at $\sim$600°C with no swelling, slight effect on tensile properties, and no effect on 650°C stress rupture properties. Electron microscopy of a V-20% Ti alloy irradiated to 1.7×10^{22} n/cm^2 at 630°C gave no evidence of any void formation.

Irradiation temperatures have not exceeded ∿650°C, but α-particle injection experiments (Ref. 12) were performed on a V-20% Nb—10% Ti alloy with tensile tests conducted at temperatures up to 950°C in order to determine the interaction between temperature and helium bubble formation. As anticipated, embrittlement was noted above ∿800°C. This basic temperature limitation, as well as lack of strength, may limit vanadium alloys to temperatures below ∿800°C.

More irradiation work is required to study fluences up to 3 x 10^{23} n/cm^2 to (1) evaluate the effects of the higher temperatures on gas-cooled reactor systems, (2) gain information on the higher-strength and contamination-resistant alloy system which might be needed, and (3) obtain information on tests in which the interactions of stress and irradiation have been observed.

3.1.5. Other Alloy Systems

Even if contamination from impurities in the coolant did not eliminate the use of vanadium alloys, both their strength and resistance to irradiation effects seem adequate only for temperatures up to about 800°C. In terms of future development, the question is whether it would be better not to pursue the vanadium alloys with this limitation, but rather to divert the development effort to alloy systems having the potential of permitting advancement to even higher-temperature operation. Alloys to be considered are chromium-, niobium-, molybdenum-, tantalum-, and tungsten-based systems. Any consideration must also include the neutronic penalties associated with their use.

3.2. FUEL-ROD DEVELOPMENT

3.2.1. Fuel-Rod Concept Evaluation

The manifolded fuel rod has been selected as the reference concept for further analysis. As discussed in the previous quarterly report (Ref. 17), this concept has a high degree of similarity to the LMFBR fuel-rod designs. Recent efforts have been concentrated on analytical models for predicting whether the in-pile performance of fuel rods will be applicable to both GCFR and LMFBR design conditions.

The fuel-cladding-interacting fuel rod utilizing a relatively heavy cladding was selected as the alternative design. Recent work has included a review of the methods being used to study the deformation and creep-collapse of the cladding as a result of the external pressure differential.

3.2.2. Creep-Collapse Analysis

During their operating lifetime, sealed fuel rods may be deformed slowly by the applied pressure differential. Excessive deformation is prevented by increasing the cladding thickness to reduce the stress in the cladding. As the cladding thickness is increased, the performance of the reactor is degraded by the addition of structural material. Hence, determining

the minimum cladding thickness to limit deformation is a design objective. The CRECOL computer code was developed as a design tool for predicting the creep-deformation of fuel cladding under reactor operating conditions. The analysis first determines the critical collapse pressure based on classical buckling for a perfectly circular tube as developed by Timoshenko and Gere (Ref. 18):

$$q_c = \frac{E_t}{4\,(1 - \nu^2)} \left(\frac{h}{r}\right)^3 \quad ,$$

where E_t = tangent modulus,

h = cladding thickness,

r = mean cladding radius,

q_c = critical collapse pressure,

ν = Poisson's ratio.

The use of the tangent modulus rather than the elastic modulus tends to lower the critical collapse pressure and allows for extension beyond the proportional limit, to the 0.2% yield stress in this case. The next step in the analysis is made by assuming that the out-of-round shape is elliptical and remains so. The assumption of an elliptical shape introduces a bending moment that is a maximum at the point of maximum curvature. The pressure stress and bending stress are added to obtain the stress distribution across the wall of the cladding. The instantaneous collapse pressure is defined as occurring when the inner compressive fiber stress rises to the 0.2% offset yield stress from the combined effect of the pressure stress and the bending stress due to the elliptical shape. Both the critical pressure and instantaneous collapse pressure are calculated independent of time.

The creep of the cladding occurs as a function of time, stress level, and temperature. For small time increments, the stresses across the cladding are assumed to remain constant and the creep strain is calculated for the time increment. Since at the apogee the compressive stress is greater at the inner surface, a greater strain occurs at this location and the radius of curvature decreases with time, resulting in an increase in ovality. The CRECOL code treats this strain as a change in the force, moment, and radius of curvature, and the stresses are recalculated for the conditions at the end of the time increment. In transforming from strain to stress, the code uses the elastic modulus rather than the tangent or secant modulus. The elastic modulus should be conservative in that it is larger than the tangent and secant moduli. The calculation proceeds by time steps, resulting in greater and greater ovality until the 0.2% offset stress is reached. The deformation is calculated to occur rapidly as it approaches the collapse stress, and the time increment is reduced

to limit the deformation to 5% of the ovality in any time interval. At present, only the material properties for Hastelloy-X and 316 SS in the unirradiated conditions are incorporated in the analysis.

The technical literature on the creep-deformation of slightly oval tubes was recently reviewed, and no approach preferable to CRECOL was identified. Hoff et al. (Ref. 19) present an analysis that is similar but simplified for hand calculation. A comparison was made of creep-collapse as calculated by their analysis and by CRECOL for the following typical fuel-rod case:

Material	Hastelloy-X
Outside radius	0.1875 in.
Wall thickness	0.020 in.
$D_{max} - D_{min}$	0.003 in.
Temperature	1400°F
Applied pressure	800 psi

The secondary creep relationship in CRECOL at 1400°F is

$$\frac{d\varepsilon}{dt} = e^{(-90.89)}\ \sigma^{8.45} \qquad 1/hr \quad .$$

For the analysis of Hoff et al., where the stress exponent must be an integer, this is adjusted to

$$\frac{d\varepsilon}{dt} = e^{(-86.7)}\ \sigma^{8} \qquad 1/hr \quad ,$$

so that the creep rates are equal at a stress of 15,000 psi. The initial stresses at the apogee as calculated by both methods are as follows:

	Inside	Outside	Average
Hoff et al.	8065 psi	6195 psi	7130 psi
CRECOL	9148 psi	5052 psi	7100 psi

These values show that both approaches calculate about the same average stress, but maximum and minimum values are more divergent in CRECOL since surface values are determined. A comparison of collapse time yields 3200 hr for the method of Hoff et al. and 1540 hr for CRECOL. Both methods calculated collapse times of the same order of magnitude, but the CRECOL values may be more accurate because CRECOL better represents the stress distribution across the cladding and also accounts for instantaneous strain and primary creep.

During the present reporting period, CRECOL was revised to break the structure up into subroutines that include calculational units and several input-output options that are designed for each type of parametric study. The subroutine OPT1 calculates the minimum wall thickness that will not collapse for specified geometry and operating conditions. For a single computation one or more wall temperatures may be specified, and the output will list a corresponding wall thickness for each temperature.

The subroutine OPT2 calculates the collapse pressure for specified geometry and operating conditions. For a single computation one or more wall temperatures may be specified, and the output will list a corresponding pressure for each temperature. The input data include a pressure range in terms of the minimum pressure and the incremental pressure to the maximum pressure.

The subroutine OPT3 calculates the collapse time for specified geometry and operating conditions. For a single computation one or more wall temperatures and one or more ovalities may be specified, and the output will list the corresponding collapse for each combination of temperature and ovality.

The shift in emphasis to the vented fuel rod (pressure balance) has imposed a lower priority on continued development of CRECOL, and further work may be postponed. The present version is sufficient for establishing a lower boundary on fuel-cladding thickness in experiments and a base to which additional cladding thickness is added as a safety factor in design studies.

Improved prediction accuracy could be obtained by performing additional work in the following areas:

1. Verifying prediction through out-of-pile experiments

2. Inputting uncertainties in material properties and outputting uncertainties in CRECOL predictions

3. Expanding the list of materials that the code has built in and expanding present built-in properties to include irradiation effects

4. Incorporating thermal stresses

5. Examining a new grid model of cladding in an attempt to assess the effect of such items as local applied force (spacer pressing against rod), nonuniform wall thickness, circumferential temperature variation, and local radius variations

6. Updating literature review to include recent European work

7. Checking the model against experiments reported in the literature (which would require generation of empirical properties for materials)

No further work is planned beyond issuing a description of the present state of CRECOL.

3.2.3. Fuel-Rod Model

Representatives from GGA attended an AEC-sponsored meeting to discuss the state of the art of analytical models used to predict the in-pile performance of fuel pins. Representatives from several other organizations involved in fast-reactor programs were also in attendance. Members of each organization described the present status of their analytical models and indicated what improvements they had planned. The BRASH, BRITL, and CRECOL programs developed at GGA were discussed by GGA personnel.

The BRASH program was written in early 1967 to investigate the fuel-cladding interactions encountered over the GCFR fuel-pin lifetime. Temperature and fuel swelling were expressed as analytic functions of time and radial position, and cladding ductility was expressed as an analytic function of time to account for radiation embrittlement. The elastic and creep deformations of the fuel and cladding were computed in determining the interaction loads, and a cumulative-damage failure criterion was employed for the cladding. A linear time variation in internal pin pressure was allowed in order to simulate gaseous fission-product buildup. Intermittent cooldown cycles during the core lifetime were accounted for in the program to investigate possible cladding yielding which might occur during cooldown. The program functioned satisfactorily, but two assumptions were made in developing the model which were somewhat questionable. The first was that the fuel pellet acts as a continuous body, when it was known that it would crack due to the high thermal stresses. The second questionable assumption pertained to the way in which fuel swelling was accommodated within the fuel matrix.

The BRITL program was written in early 1968 and was in many ways similar to BRASH, except that it accounted for radial cracks in the fuel pellets. Fuel swelling, densification or sintering, and creep are included, and the program calculates the radial temperature distribution in the fuel as a function of linear heating rate, radial fission-rate distribution, and thermal conductivity. Closing of the radial cracks due to fuel swelling and creep is allowed. BRITL has been used to calculate stresses developed in a few typical fuel-element irradiations with the assumption of linearly swelling fuel. It has also been used to interpret the applicability of fast-reactor fuel-pin irradiation data obtained in a thermal reactor.

Future work on fuel-pin modeling at GGA will include further investigation of the mechanisms of fuel swelling, creep, and porosity deployment in the fuel. Also, the effects of fast-neutron fluence on swelling and creep in the cladding will be studied. A series of sensitivity analyses are being planned to investigate the effects of variation of parameters in the mechanisms characterizing material behavior on fuel-pin performance. A modified BRITL program will be used for these studies. The analytical models developed by other organizations also will be continuously reviewed.

The CRECOL program evaluates the creep-collapse characteristics of an externally pressurized circular tube which has an initial out-of-roundness. The behavior of such a tube is dependent upon the net external pressure, the tube radius and thickness, the initial out-of-roundness, and the elastic and creep properties of the material. Several options have been incorporated into the program which allow the reactor designer to appraise the effects of several variables in order to produce a design with an adequate margin of safety. An experimental program is presently in progress to obtain more representative material-property data and to check the validity of the program.

REFERENCES

1. Okrent, D., "Neutron Physics Consideration in Large Fast Reactors," Power Reactor Tech. 7, 107 (1963-64).

2. "Liquid Metal Fast Breeder Reactor Program Plan," v. 7, "Fuels & Materials," USAEC Report WASH-1107, Argonne National Laboratory, 1968.

3. Greenberg, S., W. E. Reuther, and H. A. Levin, "Corrosion of Vanadium-Base Alloys in Sodium at 550°C to 750°C," IAEA Symposium on Alkali Metal Coolants, IAEA, Vienna, 1967, Paper SM-85/20.

4. Reuther, W. E., and D. Dorman, "Sodium Corrosion of Fuel-Jacket Alloys," in "Reactor Development Progress Report, November 1967," USAEC Report ANL-7399, Argonne National Laboratory, 1967, p. 14.

5. Greenberg, S., C. F. Cheng, and W. E. Reuther, "In-Reactor Sodium Corrosion of Vanadium and Vanadium-Titanium Alloys," Nucl. Appl. 4, 170 (1968).

6. Champeix, L., R. Darras, and J. Sannier, "Corrosion du Vanadium et de ses Alliages dans le Sodium Liquide," IAEA Symposium on Alkali Metal Coolants, IAEA, Vienna, 1967, Paper SM-85/7.

7. Gulbransen, E. A., and K. F. Andrew, "The Kinetics of the Reaction of Vanadium with Oxygen and Nitrogen," J. Electrochem. Soc. 97, 396 (1950).

8. Inouye, H., "Contamination of Refractory Metals by Residual Gases in Vacuums below 10^{-6} torr," USAEC Report ORNL-3674, Oak Ridge National Laboratory, 1964.

9. Roche, T. K., "Effect of Degree of Vacuum on the Slow-bend Creep Behavior of Columbium - 0.6% Zirconium at 1000°C," USAEC Report ORNL-3569, Oak Ridge National Laboratory, 1964.

10. Carlander, R., "The Effects of Irradiation on the Mechanical Properties of Vanadium-Base Alloys. Irradiation Effects on Reactor Structural Materials, May, June, July 1967," USAEC Report BNWL-532, Battelle Memorial Institute, Pacific Northwest Laboratory, 1967.

11. Carlander, R., "Irradiation Studies of Fuel Jacket Alloys," in "Reactor Development Progress Report, Oct. 1968," USAEC Report ANL-7513, Argonne National Laboratory, 1968, p. 91.

12. Bloom, E. E., J. O. Steigler, and F. W. Wiffen, Oak Ridge National Laboratory, unpublished data.

13. Harkness, S. D., "Examination of Irradiated Type 304 Stainless Steel and V-20 wt-% Ti by Transmission Electron Microscopy. Irradiation Effects on Reactor Structural Materials, May, June, July 1968," USAEC Report BNWL-870, Battelle Memorial Institute, Pacific Northwest Laboratory.

14. Brunhouse, J., Eidgenössiches Institut für Reaktorforschung, Switzerland, unpublished data.

15. Bohm, H., et al., "Irradiation Effects on the Mechanical Properties of Vanadium-Base Alloys," in "Effects of Irradiation on Structural Materials," American Society for Testing Materials Report ASTM STP No. 426, 1967, pp. 95-106.

16. Carlander, R., and W. F. Murphy, "Irradiation Effects on V-20 Ti and V-15 Ti-7.5 Cr Alloys," in "Irradiation Effects on Reactor Structural Materials. Quarterly Progress Report, February - April 1967," USAEC Report BNWL-455, Battelle Memorial Institute, Pacific Northwest Laboratory, pp. 3.1-3.8.

17. "Gas-Cooled Fast Breeder Reactor. Quarterly Progress Report for the Period November 1, 1968 through January 31, 1969," USAEC Report GA-9229, Gulf General Atomic Incorporated, 1969.

18. Timoshenko, S., and J. Gere, Theory of Elastic Stability, 2d ed., McGraw-Hill Book Company, New York, 1961, p. 480.

19. Hoff, N. J., W. E. Jahsman, and W. Nachbar, "A Study of Creep-collapse of a Long Circular Cylindrical Shell Under Uniform External Pressure," J. Aerospace Sci. 26, 663 (1959).

4. TASK C — TEST PROGRAM (IN-PILE AND OUT-OF-PILE TESTS)

4.1. INTRODUCTION

Data from thermal-flux capsule irradiation tests at simulated GCFR heat-generation rates, cladding temperatures, and pressure conditions are used to select fuel-rod design features and to determine parameters for future fast-flux capsule tests or loop-irradiation tests.

Thermal-flux irradiation tests have been performed on UO_2- and $(Pu-U)O_2$-fueled rods in the Oak Ridge reactor (ORR) pool-side facility (Refs. 1,2). The fuel-rod concepts under consideration are (1) sealed cans, both pressurized and nonpressurized types, and (2) manifolded, in which the fission gases diffuse to an external plenum; pressure equalization across the cladding of the manifolded fuel rods is maintained by regulating the pressure in the fission-product storage, or cleanup, system so that it is nearly equal to the primary coolant pressure.

Data on irradiation tests to date and tests being planned are summarized in Table 4.1. Information on the manifolded fuel rods, on the fast-flux tests to be conducted in EBR-II, and on the parameters to be tested during FY 70 is also presented.

4.2. IRRADIATION CAPSULE 04-P8

Examinations are being made of capsule 04-P8 (P8), in which $(Pu-U)O_2$ fueled rods reached exposures ranging from 47,000 to 59,000 MWD/tonne of heavy metal at linear heat ratings from 13.2 to 15.5 kW/ft and cladding OD temperatures from 610° to 685°C. The planned and actual irradiation conditions for capsule P8 are given in Table 4.2.

A preliminary postirradiation examination was made of the fuel-rod specimens irradiated in capsule P8. As previously reported, visual examination revealed that all three fuel rods were intact, indicating no evidence of deformation and that the rods were in excellent condition(see Fig. 4.1).

Individual gamma scans performed on each of the fuel rods revealed that the large activity peak (previously observed with the rods still in their capsule containment) corresponding to the fourth fuel pellet from the top of the lower rod (GA-19) is real in the fuel rod (see Fig. 4.2).

Postirradiation examination has also included:

1. Dimensional measurements of OD ovality, length, and bowing (see Fig. 4.3). Comparison of measurements before and after irradiation showed little or no change in dimensions except for an $\sim$3-mil ovality change in rod specimen GA-18 (see Fig. 4.3b).

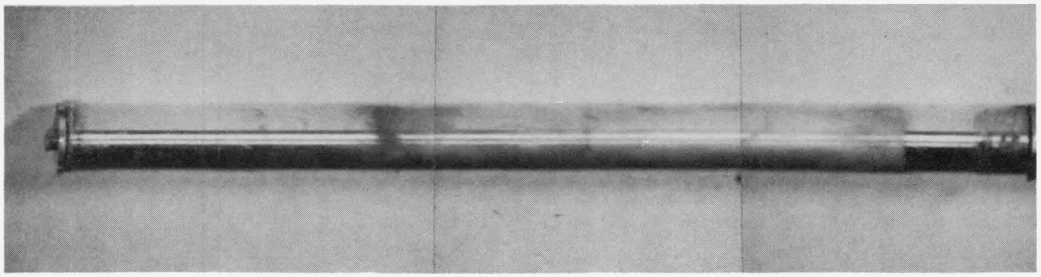

GA-17

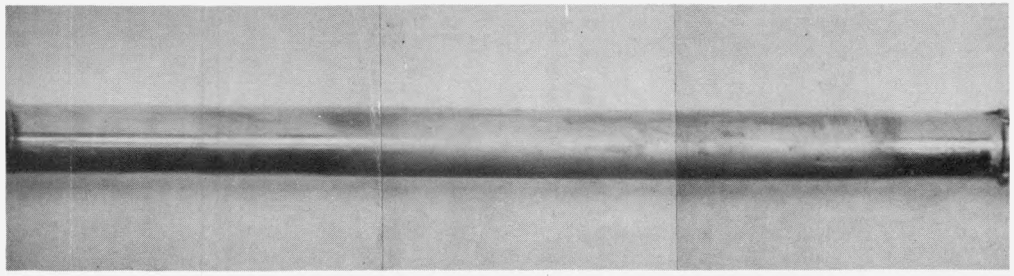

GA-18

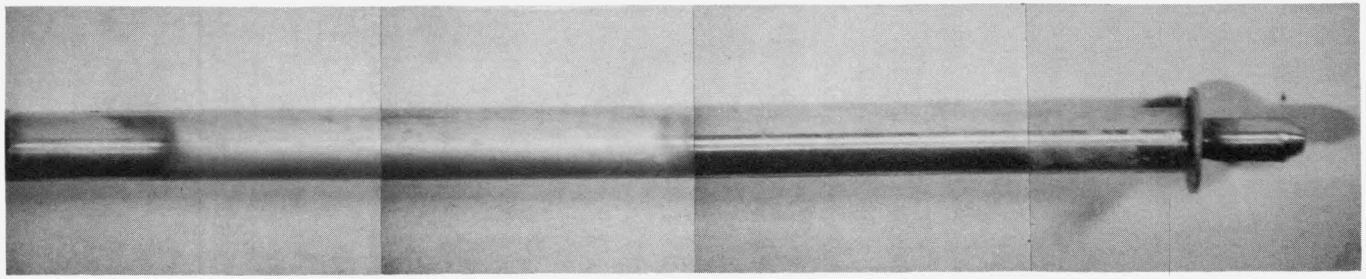

GA-19

Fig. 4.1. Photographs of fuel rods GA-17, -18, and -19 after irradiation in capsule P8 to 47,000 to 59,000 MWD/tonne of heavy metal at cladding OD temperatures ranging from 610°C to 685°C

Table 4.1

SUMMARY OF GCFR IRRADIATIONS

Test Identification	Test Reactor and Position	Schedule of Irrad. (hr)	Fuel-rod Type	Fuel-Clad. Thermal Bond	Fuel: Composition	Fuel: % TD*	Fuel: Geometry	Fuel: Stoichiometry (O/M)	Fuel: Fuel-Cladding Gap (in.)	Cladding: Composition	Cladding: Thickness OD (in.)	Conditions: Heat Rating (kW/ft)	Conditions: Max. Cladding Temperature (°F)	Conditions: Burnup (MWD/tonne) Heavy Metal	Significant Features or Results
Gulf General Atomic–Oak Ridge National Laboratory GCFR Development-Program Thermal-flux Irradiation Tests Completed															
P4-A1 GA-1	ORR-P4	650	Sealed can	He	UO_2	~90	P,A**	2.005	0.0018	Hastelloy-X	0.0091/0.379	18/21.7	1400/1490		Specimens collapsed; negl. fuel support
GA-2	ORR-P4	650	Sealed can	He	UO_2	~90	P,A	2.005	0.0028	Hastelloy-X	0.0092/0.378	18/21.7	1400/1490	3,400	
P4-B2 GA-4	ORR-P4	800	Sealed can	He	UO_2	~90	P,A	2.006	0.001/0.0025	Hastelloy-X	0.014/0.342	18/16.2	1400-1440/1250		Good condition; collapse in region of thin cladding; negligible fuel support
GA-5	ORR-P4	800	Sealed can, tapered cladding	He	UO_2	~90	P,A	2.006	0.0008/0.0023	Hastelloy-X	0.010-0.020/0.334-0.352	18/16.2	1400-1330/1250	4,500	
P4-B3 GA-6	ORR-P4	1,340	Flex-can	Na	UO_2	~95	P	2.005	0.017	304 SS	0.010/0.375	14.7	1220	5,600	Slight creep deformation
GA-7	ORR-P4	1,340	Sealed can	He	UO_2	~90	P,A	2.003	0.0036	Hastelloy-X	0.015/0.343	12.1	1220	5,700	
P4-B4 GA-8	ORR-P4	2,000	Flex-can	Na	UO_2	~95	P	2.0032	0.015	304 SS	0.010/0.375	13.5/15.1	1300/1390	8,300	Good collapse stability
GA-9	ORR-P4	2,000	Sealed can,PP†	He	UO_2	~90	P	2.0032	0.0036	Hastelloy-X	0.015/0.343	11.4/12.6	1200/1320	8,800	
O4-P5 GA-10	ORR-O4	2,200	Sealed can,PP	He	UO_2	~90	P,A	2.0039	0.0035	Hast.-X partially surface-roughened	0.015/0.343	14.0	1310	11,000	Some cladding deformation under thermocouple used to monitor temperature of OD
GA-11	ORR-O4	2,200	Sealed can,PP	He	UO_2	~90	P,A	2.002	0.0035	Hast.-X partially surface-roughened	0.015/0.343	16.2	1500	12,000	Good collapse stability
GAL-1 ORR Exp 16	ORR Loop	~4 total	Sealed can	He	UO_2	~90	P,A	2.003	0.003	Hast.-X partially surface-roughened	0.015/0.343	16	1500	~10	
O4-P6 GA-12	ORR-O4	1,100	Sealed can	He	88 UO_2–12 PuO_2	~90	P,A	1.98/1.99	0.0033	Hast.-X partially surface-roughened	0.015/0.343	15	1310	4,200	Good collapse stability
GA-13	ORR-O4	1,100	Sealed can	He	88 UO_2–12 PuO_2	~90	P,A	1.98/1.99	0.0033	Hast.-X partially surface-roughened	0.015/0.343	18	1500	4,800	Collapsed into oval shape; negligible fuel support
GA-14	ORR-O4	1,100	Sealed can,PP	He	88 UO_2–12 PuO_2	~90	P,A	1.98/1.99	0.0033	Hast.-X partially surface-roughened	0.015/0.343	18	1540	4,800	Cladding failed under thermocouple band; negligible fuel support
O3-P7 GA-15	ORR-O3	~7,800	Sealed can	He	UO_2	~90	P,A	2.002	0.0025	Hastelloy-X	0.020/0.353	6.8	1400	~16,000	Irradiation discontinued at 16,000 MWD/tonne
GA-16	ORR-O3	~7,800	Sealed can	He	88 UO_2–12 PuO_2	~90	P,A	1.98/1.99	0.0034	Hastelloy-X	0.020/0.353	8.2	1400	~16,000	Fission-product leak detected in rod
O4-P8 GA-17	ORR-O4	~11,000	Sealed can	He	88 UO_2–12 PuO_2	~90	P,A	1.98/1.99	0.002	316 SS	0.024/0.355	13.2	1150	~47,000	
GA-18	ORR-O4	~11,000	Sealed can	He	88 UO_2–12 PuO_2	~90	P,A	1.98/1.99	0.003	Hastelloy-X	0.015/0.343	15.5	1300	~59,000	Fuel-rod specimens all in excellent condition; little, if any, deform. observed
GA-19	ORR-O4	~11,000	Sealed can,PP	He	88 UO_2–12 PuO_2	~90	P,A	1.98/1.99	0.003	Hastelloy-X	0.015/0.343	15.5	1300	~59,000	
Gulf General Atomic GCFR Development-Program Irradiation Tests Planned															
Thermal-flux Tests															
O4-P9	ORR	~11,000	Manifolded to external plenum	He	88 UO_2–12 PuO_2	~90	P,A	~1.98	~0.003-0.004	316 SS	0.024/0.355	15	1300	>50,000	Fission-product emission at top of fuel rod and top of fission-product trap will be monitored; instrumented rod and trap; rod external pressure ~950 psi, internal pressure ~1000 psi under normal operating conditions.
Fast-flux Tests															
F-1 Subassembly (7 or 19 rods)	EBR-II	~10,000	Manifolded to ext'nl plenum	He	88 UO_2-15 PuO_2	~90	P, A	~1.98	~0.002-0.003	316 SS	OD/ID ~1.15	12 - 16	1300-1470	>50,000	Not instrumented; ambient pressure
F-2 Subass'y (7, 19 rods)	EBR-II	~10,000 to 20,000	Manifolded to ext'nl plenum and sealed can	He	88 UO_2-15 PuO_2	~90	P, A V††	~1.98	~0.002-0.003	316 SS Hast.-X (sealed can only)	OD/ID ~1.15	12 - 16	1300-1470	>50,000	Not instrumented, ambient pressure. Some sealed rods with high-strength cladding may also be included.

*Smear density was less than or equal to 85% of theoretical.
** Pellet, annular.
†PP = Prepressurized rod (external pressure 800 to 1000 psi in capsules, 300 psi in loop).
††Vibratory compacted.

Table 4.2

IRRADIATION CONDITIONS FOR CAPSULE P8

Parameters	Fuel-rod Specimens					
	GA-17		GA-18		GA-19	
	Planned	Actual	Planned	Actual	Planned	Actual
Fuel	$(Pu-U)O_2$	[88 U(9% enr) - 12 Pu]O_2	$(Pu-U)O_2$	[88 U (9% enr) - 12 Pu]O_2	$(Pu-U)O_2$	[88 U (9% enr) - 12 Pu]O_2
Fuel smear density, % TD	$\leq$85	80.0	$\leq$85	82.7	$\leq$85	83.8
Cladding material	←316 stainless steel→		←Hastelloy-X→		←Hastelloy-X→	
Cladding surface	←Smooth→		←Smooth→		←Smooth→	
Inner sleeve material	←Incoloy 800→		←Incoloy 800→		←Inconel 625→	
Shim-rod material	←316 stainless steel→		←Hastelloy-X→		←Hastelloy-X→	
Bond-gap fluid	←Helium→		←Helium→		←Helium→	
Initial cladding pressure differential, hot, psig	←970→		←970→		←500→	
External rod pressure, psig	←1,000→		←1,000→		←1,000→	
Clad surface temp., °C (max)	700	610†	700	685	700	685
Linear heating rate, kW/ft	16	13.2*	16	15.5*	16	15.5*
Irradiation time, hr	10,000	11,000	10,000	11,000	10,000	11,000
Burnup, MWD/T	50,000	47,000*	50,000	59,000*	50,000	59,000*
Power/temperature cycling	----	59	----	59	----	59
Pressure cycles, 1000 - 100 - 1000 psig	----	20	----	20	----	20

*Based on thermal analysis.

†Temperature on OD of rod specimen GA-17 swung from 560° to 660°C during each ORR cycle.

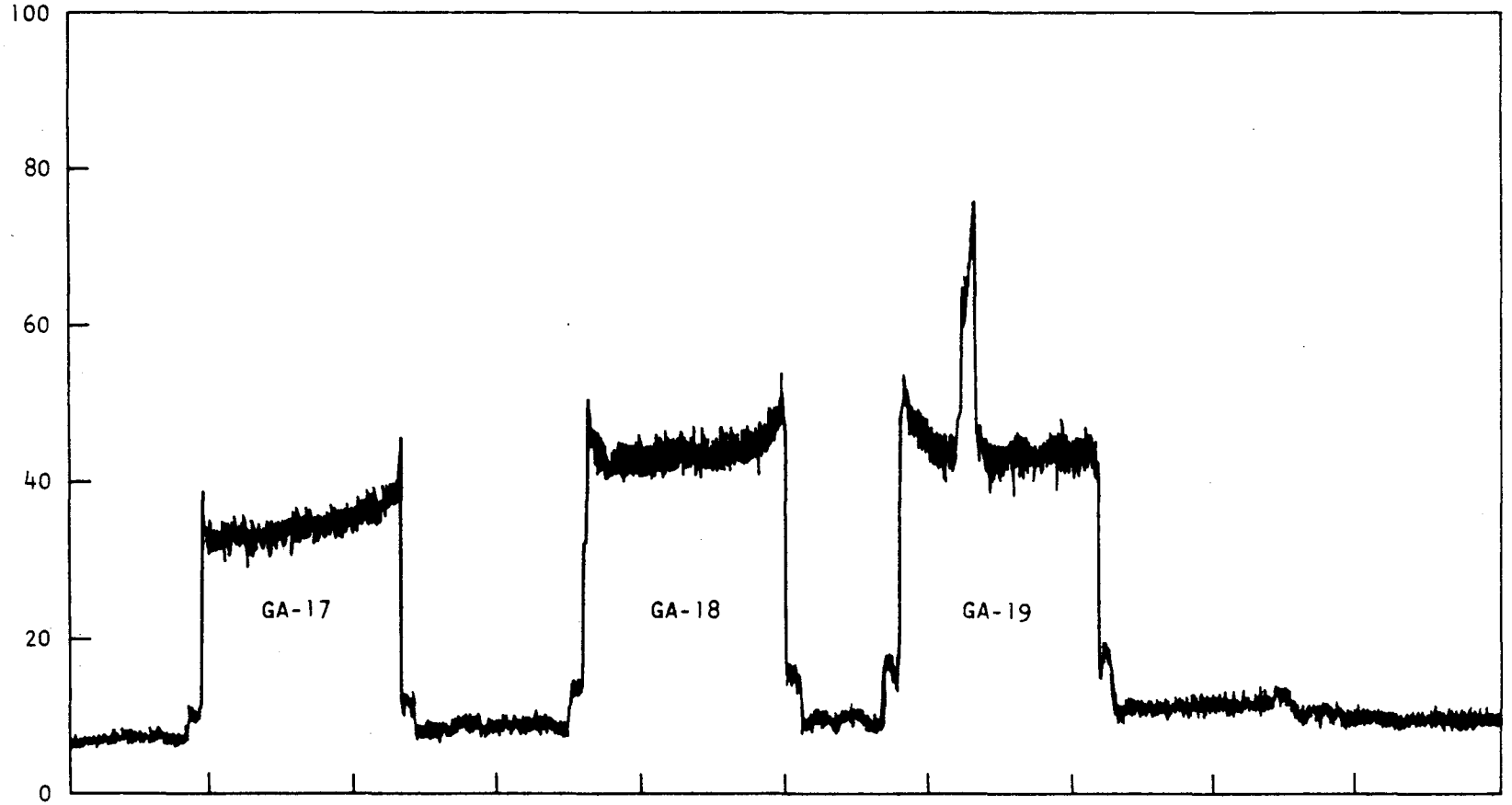

Fig. 4.2. Gross gamma scan of individual fuel rods irradiated in capsule P8 after rods were removed from the capsule containment

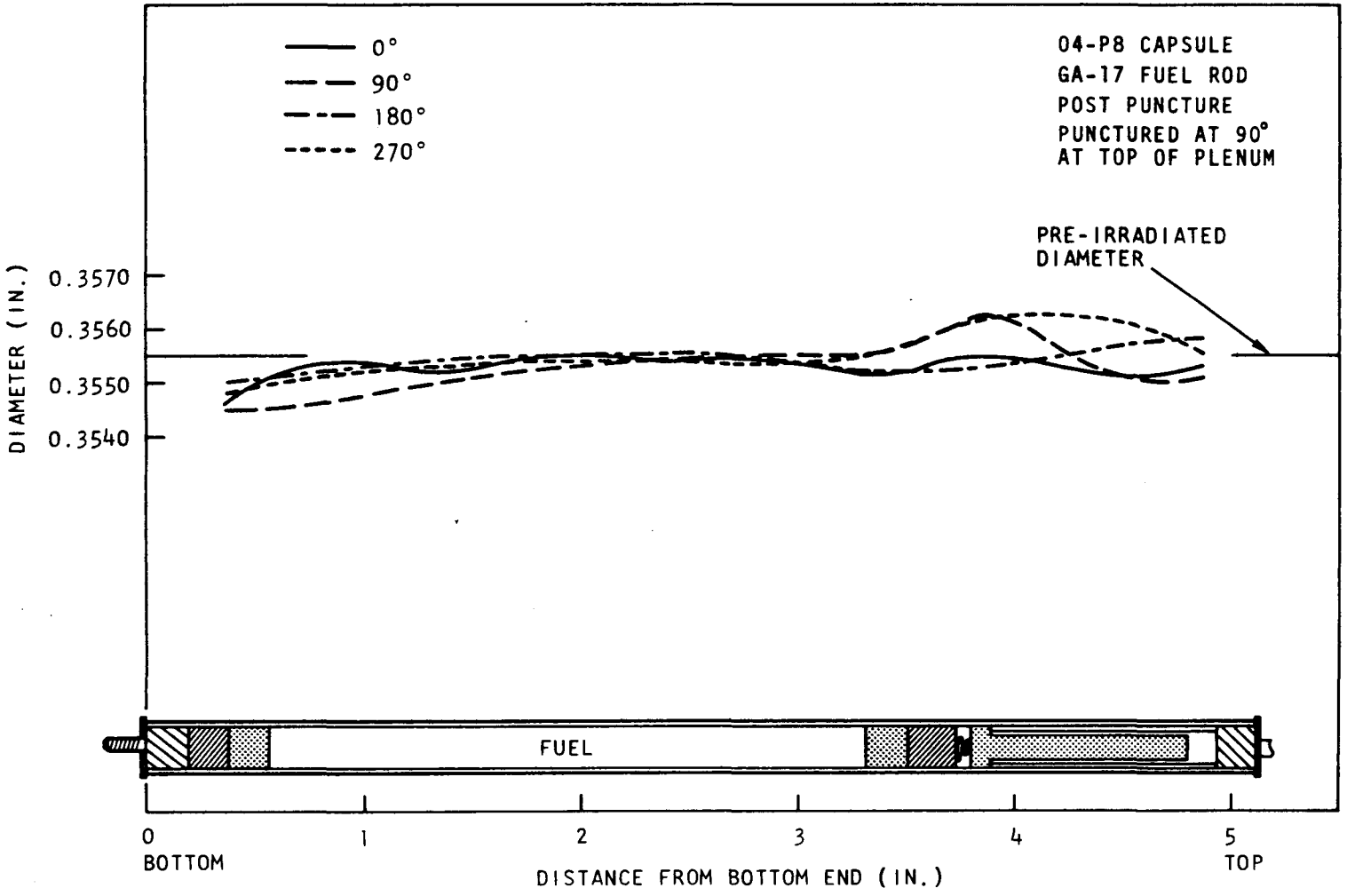

Fig. 4.3a. Plot of preirradiation and postirradiation diametral measurements made on fuel-rod specimen GA-17, capsule P8

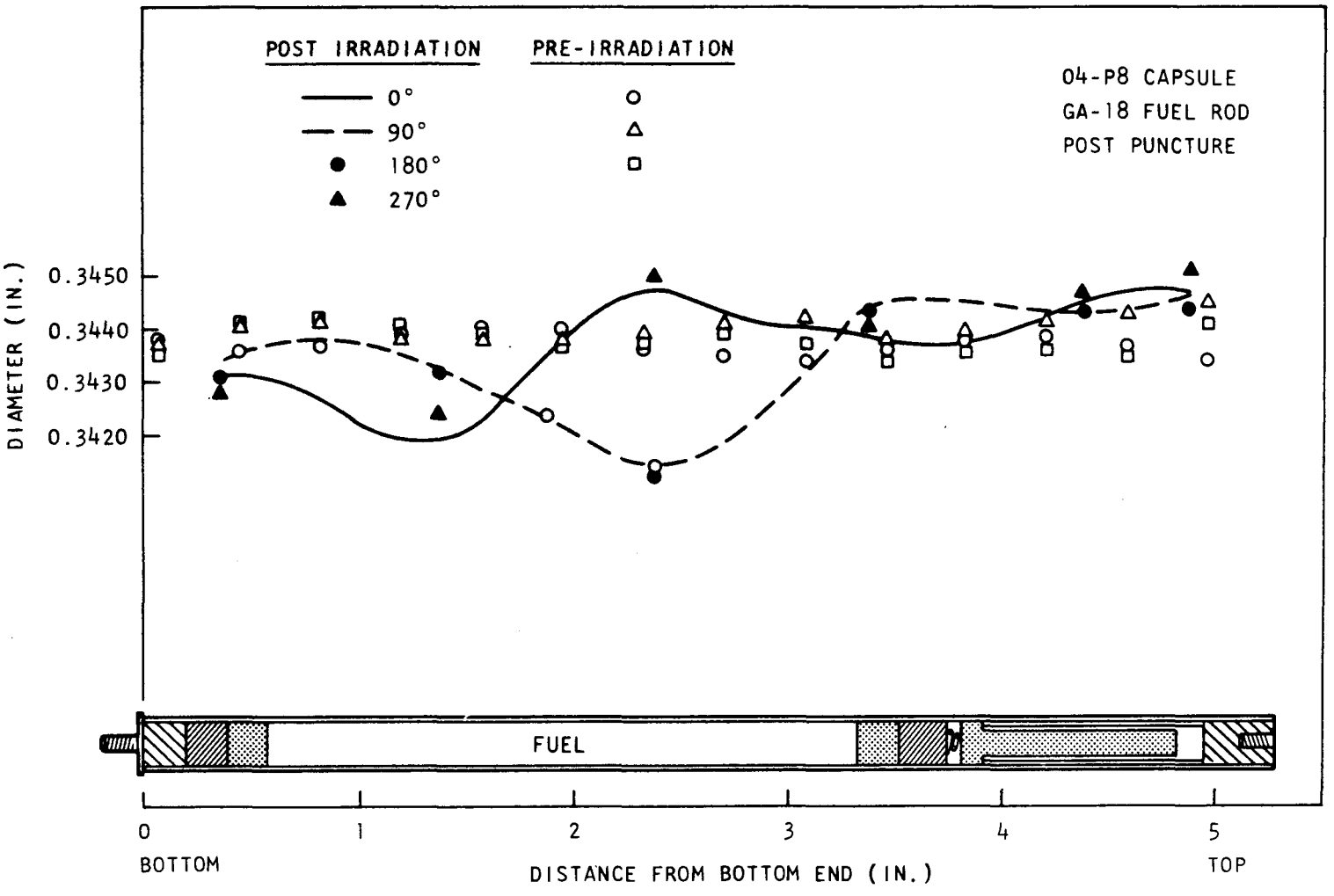

Fig. 4.3b. Plot of preirradiation and postirradiation diametral measurements made on fuel-rod specimen GA-18, capsule P8

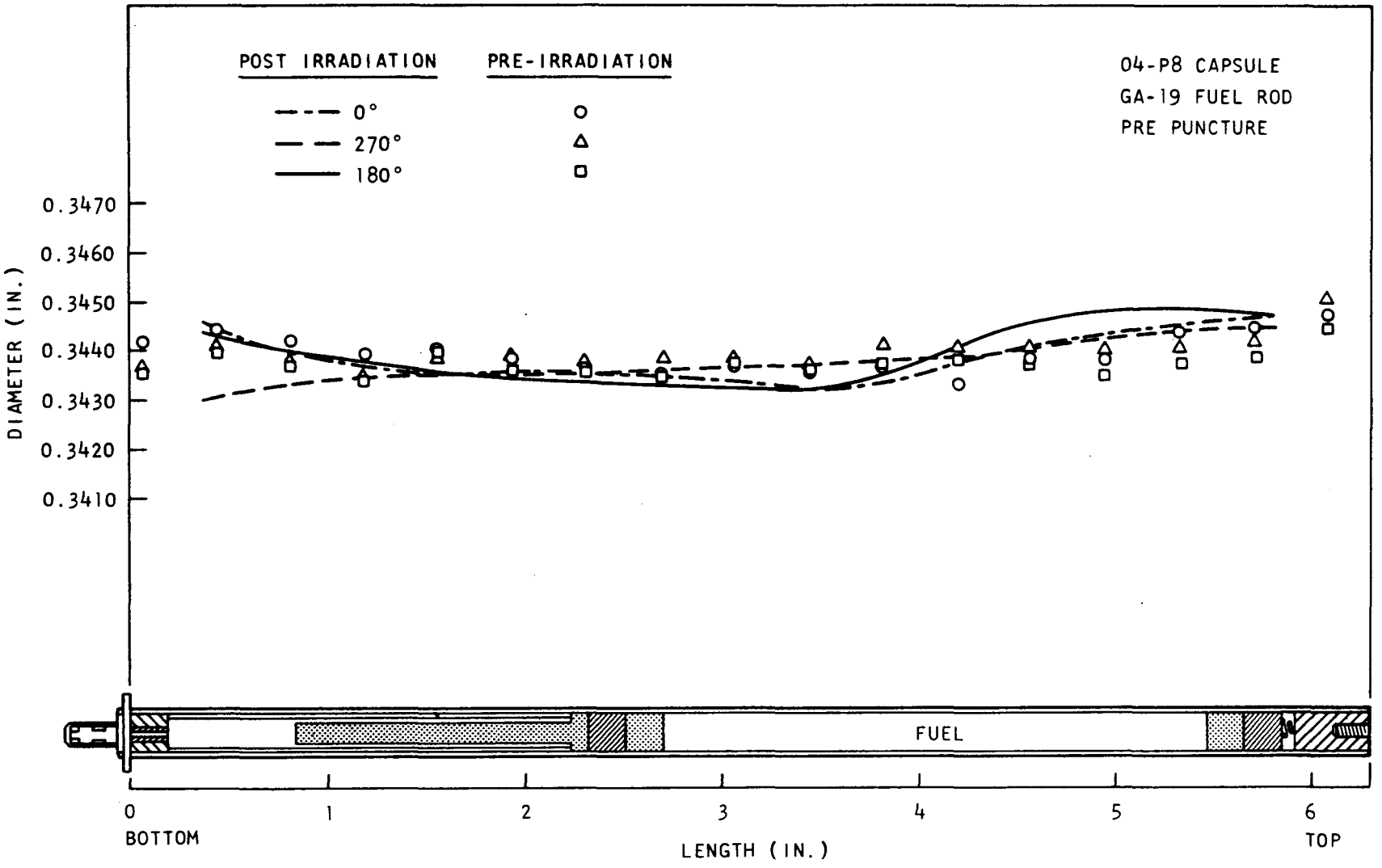

Fig. 4.3c. Plot of preirradiation and postirradiation diametral measurements made on fuel-rod specimen GA-19 (prepressurized), capsule P8

2. Fission-gas-release measurements. The fuel-rod plenums were punctured and the total gas content was determined (the accuracy of the volume measurement needs to be determined); the gases are now being analyzed and identified. Fractional fission-gas-release values will be determined when the analyses are complete. Cladding dimensions were rechecked after puncturing to determine whether cladding strain corresponded to the gas pressure. However, the changes observed were so small that they were in the range of the accuracy of the equipment.

Further postirradiation examination will include:

1. Burnup analysis. Representative pellets from each rod will be analyzed (see Fig. 4.4).

2. Neutron dosimetry-wire analysis

3. Metallographic examination. Representative transverse and longitudinal sections (see Fig. 4.4) from each fuel rod will be examined, and a microprobe analysis will be performed where such a requirement is indicated (e.g., to determine the identity of diffusing components involved in fuel-cladding–fission-product chemical interactions.

4. Mechanical-property tests. These will be made to determine radiation effects on the 316 SS and Hastelloy-X fuel-rod claddings, and cladding specimens of Incoloy 800 and Inconel 625 will be scheduled for tests after 10,000-hr aging of control specimens. The aging will be performed at temperatures corresponding to the cladding temperatures indicated during the irradiation test. Mechanical-property tests will be of the ring-pull type and will be performed at temperatures ranging from room temperature to 800°C.

4.3. FUTURE IRRADIATION TESTS

Irradiation test work planned for the next reporting period will include the following:

1. Fabrication of the manifolded fuel-rod specimen for the capsule 04-P9 thermal-flux (ORR) test will be completed, and the irradiation will be initiated.

2. Overall design of the subassembly (F1) for fast-flux testing in EBR-II will be continued. The design and planning of the seven or 19 fuel-rod specimens (in which the pressure differential is kept low as would be experienced in a manifolded fuel rod) will be completed.

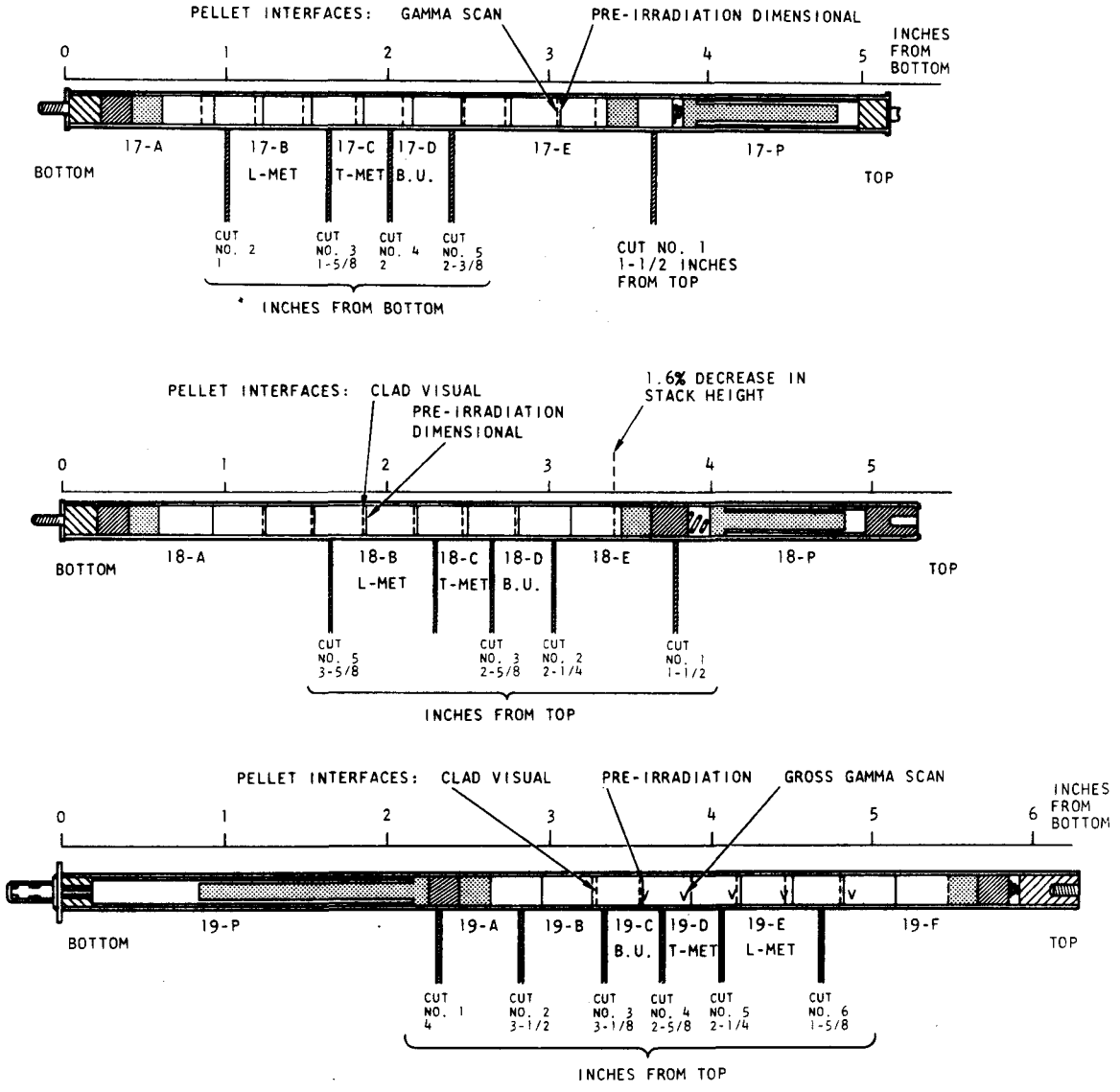

Fig. 4.4. Illustration of locations from which metallographic examination and burnup analysis samples were cut from fuel-rod specimens, capsule P8

Details of the work completed and planned on the thermal-flux irradiation of capsule O4-P9 are given in Section 4.3.1; details of the work on fast-flux irradiation capsule F-1 are given in Section 4.3.2.

4.3.1. Irradiation Capsule O4-P9

Capsule O4-P9 (P9) will contain one fuel rod, of the manifolded (to external plenum) fuel-rod concept. This rod will be operated over a long irradiation period with exposure to >50,000 MWD/tonne burnup at a linear heat-generation rate of 15 kW/ft. The rod will have a maximum cladding outer surface temperature of 700°C and will contain a fission-product trap which will operate with an outer surface temperature of ∿300°C. The design layout of the fuel-rod specimen is shown in Fig. 4.5, and a schematic of the revised fission-product-trap monitoring system is shown in Fig. 4.6. A layout of the capsule design is shown in Fig. 4.7. The planned test conditions for capsule P9 are given in Table 4.3. The numbers and types of power and pressure cycles (and the monitoring tests required) are listed in Table 4.3; steady-state test conditions are also listed. The trap and blanket regions are electrical-resistance-heated to allow control of cladding OD temperatures of ∿300°C in those regions.

4.3.1.1. Fabrication. Fabrication and characterization of the cladding, blanket, monitoring tube, trap thermocouple, trap charcoal, and insulator materials for the GA-20 fuel rod have been completed, and a preliminary assembly of the cladding components, instrumentation, and trap has been made. ORNL is currently performing ultrasonic and eddy-current testing of the fuel-rod cladding. It is expected that the assembly, except for insertion of the fuel and final end closure, and the characterization of the actual components will be completed in June 1969.

ORNL has obtained the plutonium and prepared the powders required for the fuel and has prepared some trial pellets. Pellet fabrication is expected to begin as soon as trial pellets have been characterized to determine the sintering characteristics of the fuel.

4.3.1.2. Experimental Studies. Laboratory experiments pertaining to the release of noble gases from the GCFR fuel element are under way. Two basic parameters are being measured: (1) the diffusion coefficient, D_{12}, for the gas pairs krypton-helium and xenon-helium, and (2) the adsorption coefficient, K', for krypton and xenon on activated carbon. These data provide input to computer calculations (see Section 4.3.1.3) for estimation of diffusion delay times and therefore fission-product-release fractions from either the prototype fuel element or proposed vented capsules such as P9.

In the diffusion experiments, a mockup of the P9 capsule is used. The apparatus is a 0.307-in.-ID, 19.7-in.-long steel tube, with a source of Kr^{85} provided at the bottom and an ionization chamber located at the top. The experimental procedure involves introducing the krypton source (Kr^{85} mixed with helium at the same total pressure as the test capsule) at the bottom and continuously monitoring the buildup of activity at the top. Tests have been made on the empty tube and on the tube loaded with simulated

NOTES:

1. ALL DIMENSIONS EXCEPT OVERALL DIMENSIONS ARE REFERENCE & NOMINAL
2. SELECT PELLETS PER SPEC. 393-5002
3. ASSEMBLE PER SPEC. 393- _____
4. ITEM 10 POSITIONED BY ROLLING METHOD OR BY "MAGNA-FORM"

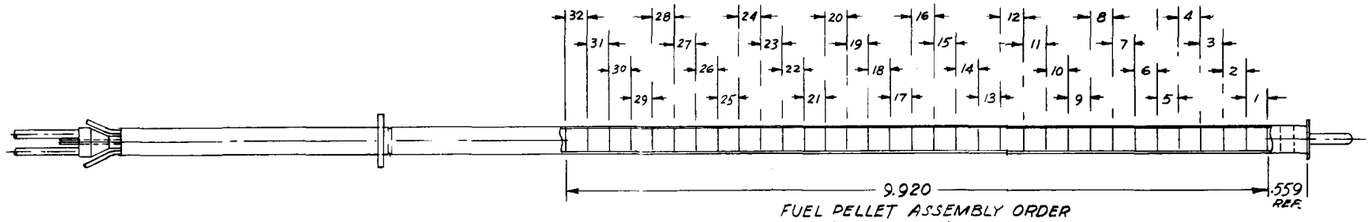

FUEL PELLET ASSEMBLY ORDER
(ACTUAL SIZE)

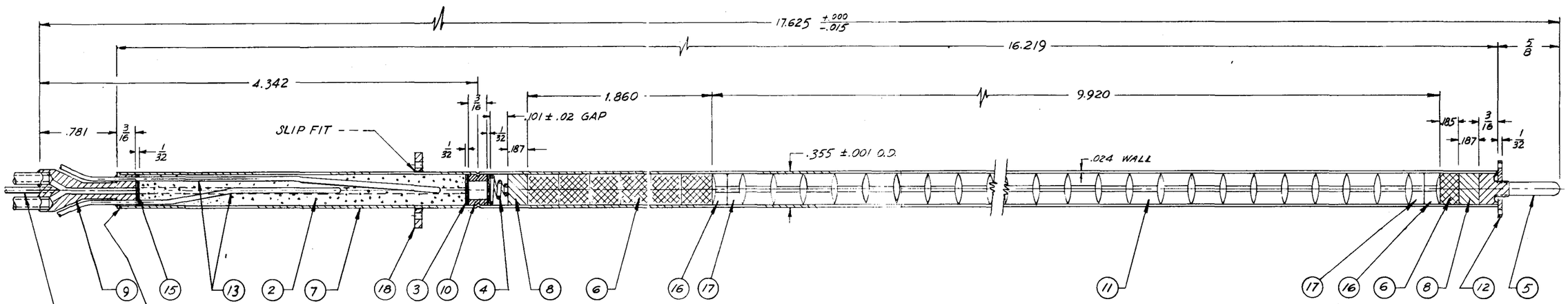

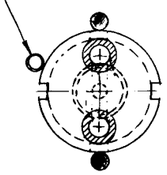

TOP END VIEW
4/1

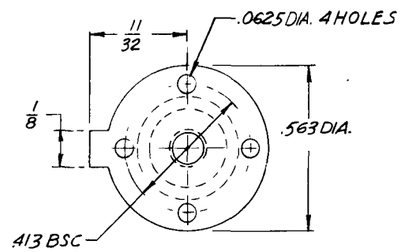

LOWER END VIEW
4/1

DIMENSIONS IN INCHES
SCALE 2/1 & NOTED

						1	18	-201-14	LOCATING COLLAR		
						2	17	-201-12	SUPPRESSOR PELLET		
						2	16	-201-11	SUPPRESSOR PELLET		
						1	15	-201-13	SCREEN		
						X	14	-	F.P. TUBE 1/16 O.D. .011 WALL	SSTL	316
						2	13		THERMO COUPLE 1/16 O.D.	SST. CLAD S/A	
						1	12	-201-6	BOTTOM LOCK		
						32	11	-201-1	FUEL PELLET		
						1	10	-201-10	SPACER PLUG		
						1	9	-201-7	END PLUG		
						2	8	201-3	INSULATOR		
						1	7	-201-5	CLADDING TUBE		
						7	6	-201-4	BLANKET PELLET		
						1	5	-201-8	END PLUG		
						1	4	-201-2	SPRING		
						2	3	393-5413-201-9	SCREEN		
						X	2		ACTIVATED CHARCOAL	BARNABY CHANEY	IM
							1	-1	ASSEMBLY		

Fig. 4.5 Detail of parts for capsule P9 (Part 1)

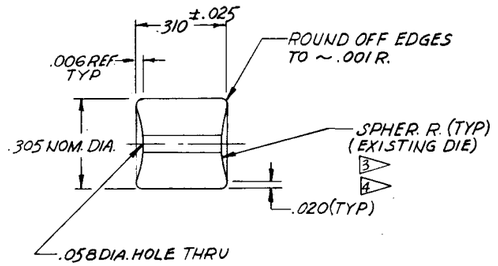

(1)

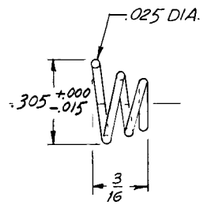

(2)

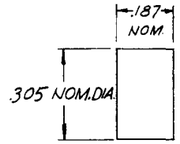

(3)

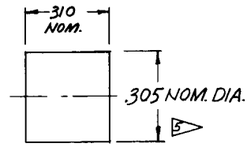

(4)

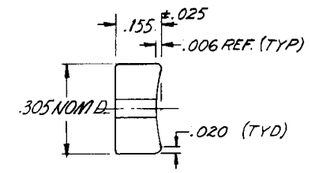

(11) (12)

NOTES:

1. REMOVE ALL BURRS & SHARP EDGES.
2. DIA. OF FUEL PELLETS TO BE .003 TO .005 LESS THAN THE MEASURED AVERAGE TUBE I.D. TOLERANCE ON FINISHED PELLET TO BE ±.0005. METHOD OF MEAS. TUBE I.D. TO BE IN ACCORDANCE WITH SPEC. 393-5001
3. USE EXISTING DIE GGA TOOL NO. 393-DH-275
4. FUEL PELLETS TO BE FABRICATED IN ACCORDANCE WITH SPEC. 393-3007
5. USE EXISTING DIE GGA TOOL NO. 393-F-280.
6. TUBE I.D. TO BE MEASURED PER SPEC. 393-5001 TUBE WALL THICKNESS TO BE MEASURED PER SPEC. 393-5003.
7. MAKE FROM .375 O.D. X .031 WALL TUBE. GRIND OUTSIDE DIA. ON A HARDENED STEEL MANDRIL TO DIMENSION SHOWN.
8. TOLERANCE SYMBOLS PER MIL-STD-8.
9. DIA. TO BE .0005 -.001 SMALLER THAN MEAS. I.D. OF ITEM (5).

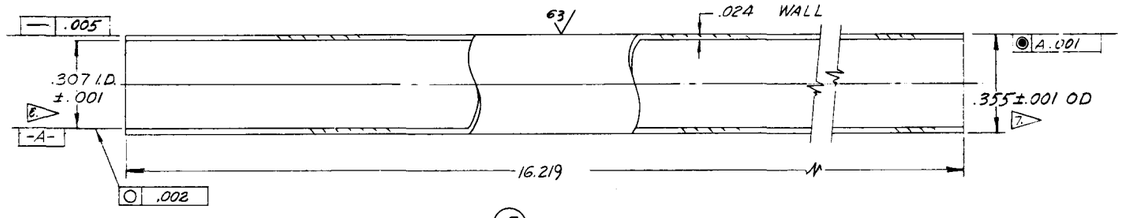

(5)

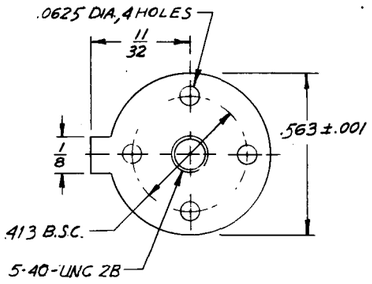

(6)

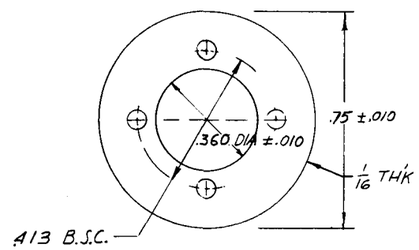

(14)

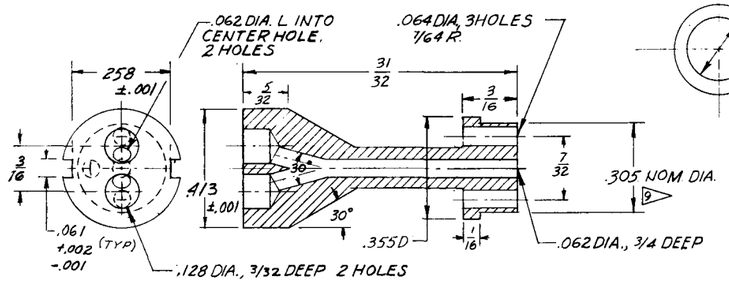

(7)

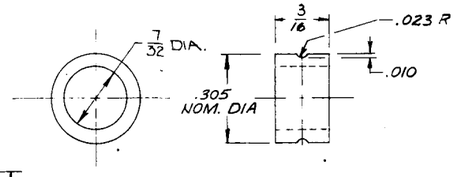

(10)

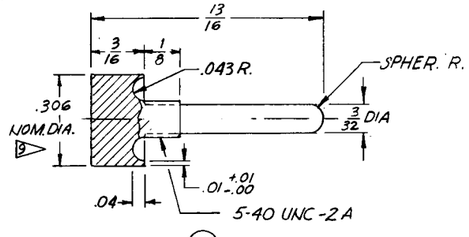

(8)

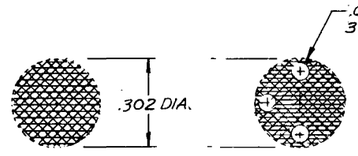

(9) (13)

	14		LOCATING COLLAR	SST-304	
	13		SCREEN	SST-316	30-40 MESH
	12		SUPPRESSOR PELLET	8.3% Enr UO_2	393-2016
	11		SUPPRESSOR PELLET	14.9% Enr UO_2	393-2016
	10		SPACER PLUG	ST STL-316	393-2014
	9		SCREEN	ST STL-316	30-40 MESH
	8		END PLUG	ST STL-316	393-2013
	7		END PLUG	ST STL-316	393-2013
	6		BOTTOM LOCK 1/32 THK	ST STL-304	
	5		CLADDING TUBE	ST STL-316	393-2015
	4		BLANKET PELLET	NAT UO_2	393-2009
	3		INSULATOR PELLET	AL_2O_3	393-2008
	2		SPRING	INCONEL	718. 393-3017
	1		FUEL PELLET	PUO_2-UO_2	393-2012

Fig. 4.5 Detail of parts for capsule P9 (Part 2)

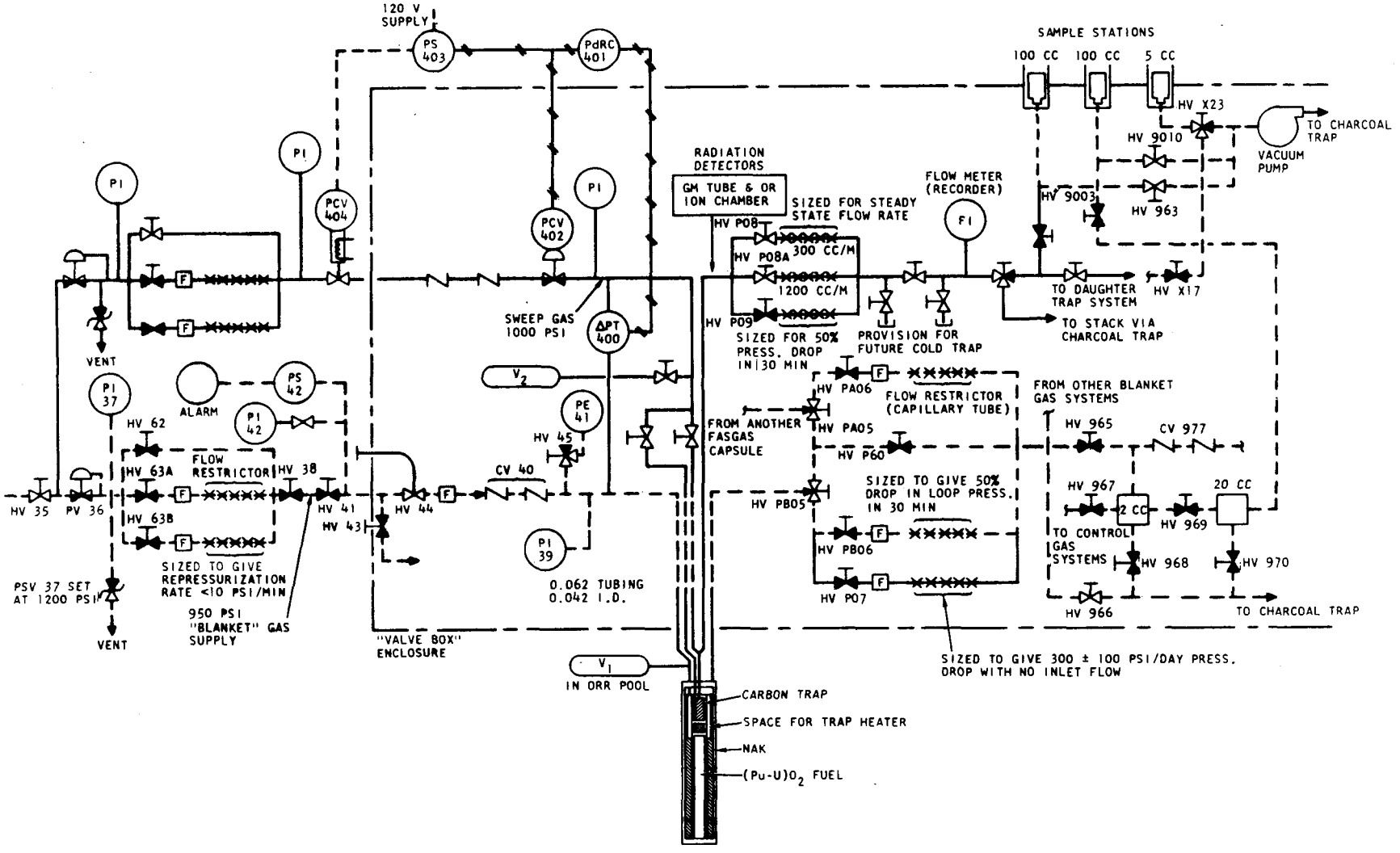

Fig. 4.6. Diagram of fission-product-trap monitoring system for capsule P9

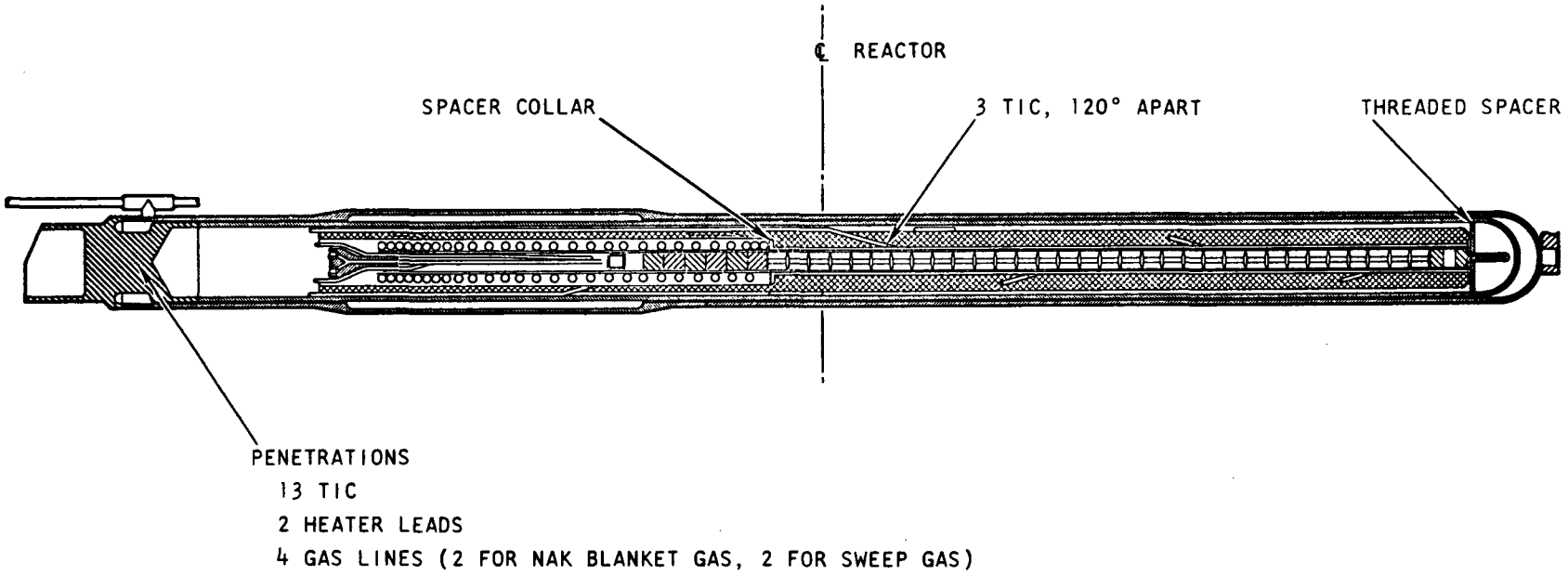

Fig. 4.7. Capsule P9 design

Table 4.3

PLANNED IRRADIATION TEST CONDITIONS FOR CAPSULE P9

Rod specimen	GA-20
Cladding material	316 SS
Cladding OD, in.	0.355
Cladding thickness, in.	0.024
Cladding OD/ID	1.156
Bond-gap fluid	Helium
Cladding OD surface temperature, °C	700 + 0, - 25
Fuel	[88 U (9% enr)—12 Pu]O_2
Fuel smear density, % TD	$\leq$85
Linear power generation (max.), kW/ft	15 ±2
Burnup exposure, MWD/tonne	$\geq$50,000 (15 x 10^{20} f/cm^3)
External pressure, psig	950 ±25
Initial internal trap pressure, hot, psig	1000 ±25
End-of-life internal trap pressure, hot, psig	1000 ±25
Trap temperature surface, °C	300 ±50
Pressure differential trap wall, psi	50, nominal; not to exceed 300
Number of power (temperature) cycles	100 standard (700°C → 300°C → 700°C); 6 nonstandard (700°C → x → 700°C)
Number of pressure cycles	20 standard (1000 psig → 100 psig → 1000 psig); 9 nonstandard (1000 psig → x → 1000 psig)

fuel and blanket pellets and/or the carbon trap. The carbon trap consists of 1.7 g of Barnaby-Cheney MI-6736 10-20 mesh held in place with screens. Helium pressures of 14.7 psia, 165 psia, and 1010 psia have been utilized. Although only room-temperature tests have been performed thus far, experiments at temperatures to 400°C are planned.

The results of the first nine experiments are presented in Ref. 1. The results of six subsequent tests are shown in Fig. 4.8, where C/C_{max} (or fraction of final equilibration) is plotted as a function of time. Table 4.4 contains the experimental conditions for these runs. The experimental curves in Fig. 4.8 are presently being analyzed by computer calculations using the SLIDER code. Some tentative results of these calculations are given in Section 4.3.1.3.

Table 4.4

CONDITIONS FOR DIFFUSION OF KRYPTON IN CAPSULE P9 MOCKUP AS SHOWN IN FIG. 4.8

Run No.	Temp.	Helium Pressure (atm)	Loading
9	RT	69.5	1.7 g (8 cm) MI-6736 charcoal + blanket pellets (5.2 cm)
10	RT	1.0	1.7 g (8 cm) MI-6736 charcoal + blanket pellets (5.2 cm)
11	RT	11.2	1.7 g (8 cm) MI-6736 charcoal + blanket pellets (5.2 cm)
12	RT	35	1.7 g (8 cm) MI-6736 charcoal + blanket pellets (5.2 cm)
13	RT	1.0	None (empty tube)
14	RT	69.5	None (empty tube)
15	RT	69.5	None (empty tube)

The second phase of the out-of-pile experiments involves determination of the adsorption isotherms for xenon and krypton on carbon at elevated temperatures. The technique used is the ordinary manometric procedure whereby a known amount of the adsorbate is admitted to the adsorbent, which is maintained at the temperature of interest. From pressure-volume measurements, the amount adsorbed, Q, is calculated.

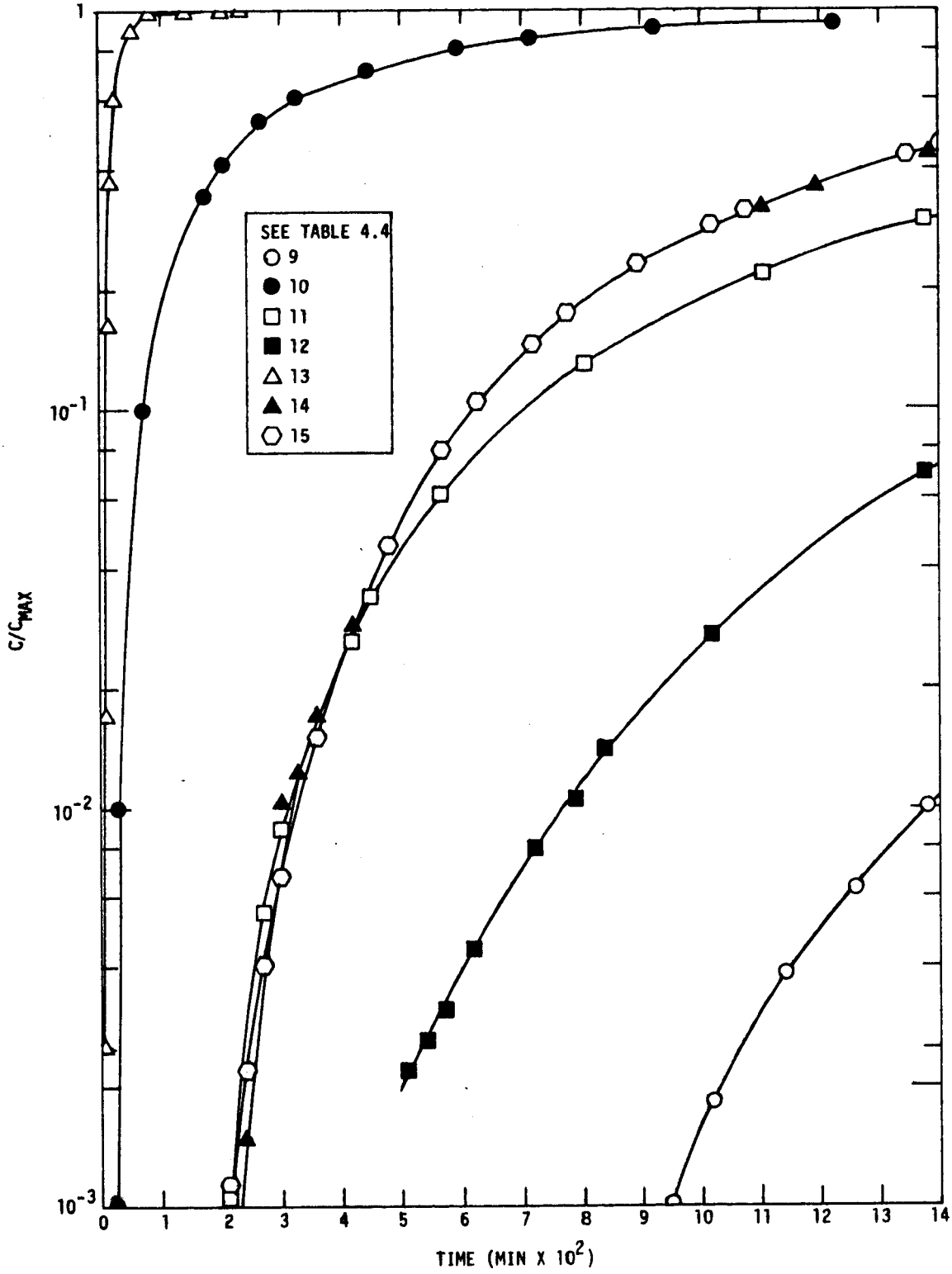

Fig. 4.8. Diffusion of krypton in capsule P9 mockup plotted as C/C_{max} versus time

Complete adsorption isotherms for xenon on carbon (Barnabey-Cheney MI-6736, 10-20 mesh) are given in Ref. 1. Complete isotherms for krypton on carbon are given in Fig. 4.9, where the amount sorbed, Q, is plotted versus equilibrium krypton pressure (in mm Hg). The adsorption coefficient, K', is the slope of the isotherm, where P is in atmospheres. Thus, K' is equal to Q at the equilibrium sorbate pressure of 1 atm.

An additional series of experiments was performed to measure the effect of total helium pressure on the krypton adsorption coefficient. In these tests a dynamic technique was used in which the time for a pulse of Kr^{85} to traverse a small bed of carbon was measured. K' was then calculated from the relation $t = K' V/F$, where t is the delay time (min), V is the carbon volume (cm^3), and F is the flow rate (cm^3/min). Tests were performed at several flow rates and at total helium pressures of 1, 10, and 70 atm. K' was found to be essentially constant at all of these pressures. This result is somewhat at variance with the expected result (based on previous experiments) that high helium pressure should inhibit, by competitive adsorption, the adsorption of other species.

4.3.1.3. Analysis of Krypton Diffusion Experiments. Analysis of krypton diffusion experiments is being conducted using the SLIDER computer program. The results of the analysis of runs 1, 3, 13, and 17 are presented in Fig. 4.10, where the experimental data and curves are plotted and compared with various assumed diffusion coefficients. For pressures of 1, 10.5, and 11.2 atm, the results verify the values of the diffusion coefficients computed from the Hirschfelder, Curtis, and Byrd equation. For example, the room-temperature, 1.0-atm value is 0.665±0.01 as compared with a value of 0.65 derived from the equation.

A check was made of the capability of SLIDER to yield valid results for this analysis. The time-dependent analytical solution for the SLIDER representation of run 1 was found to be

$$C(t)/C(\infty) = 1 + \frac{2b}{\pi a} \sum_{n=1}^{\infty} \frac{(-1)^n}{n} \cdot \sin\left(\frac{n\pi a}{b}\right) \cdot e^{-(\pi^2 n^2 D/b^2)t} ,$$

where $C(t)$ = concentration at the end of the diffusion tube at any time t,

$C(\infty)$ = concentration at the end of the diffusion tube after infinite time,

a = outer boundary dimension of the initial source region,

b = outer boundary dimension of the diffusion tube,

D = diffusion coefficient (cm^2/sec).

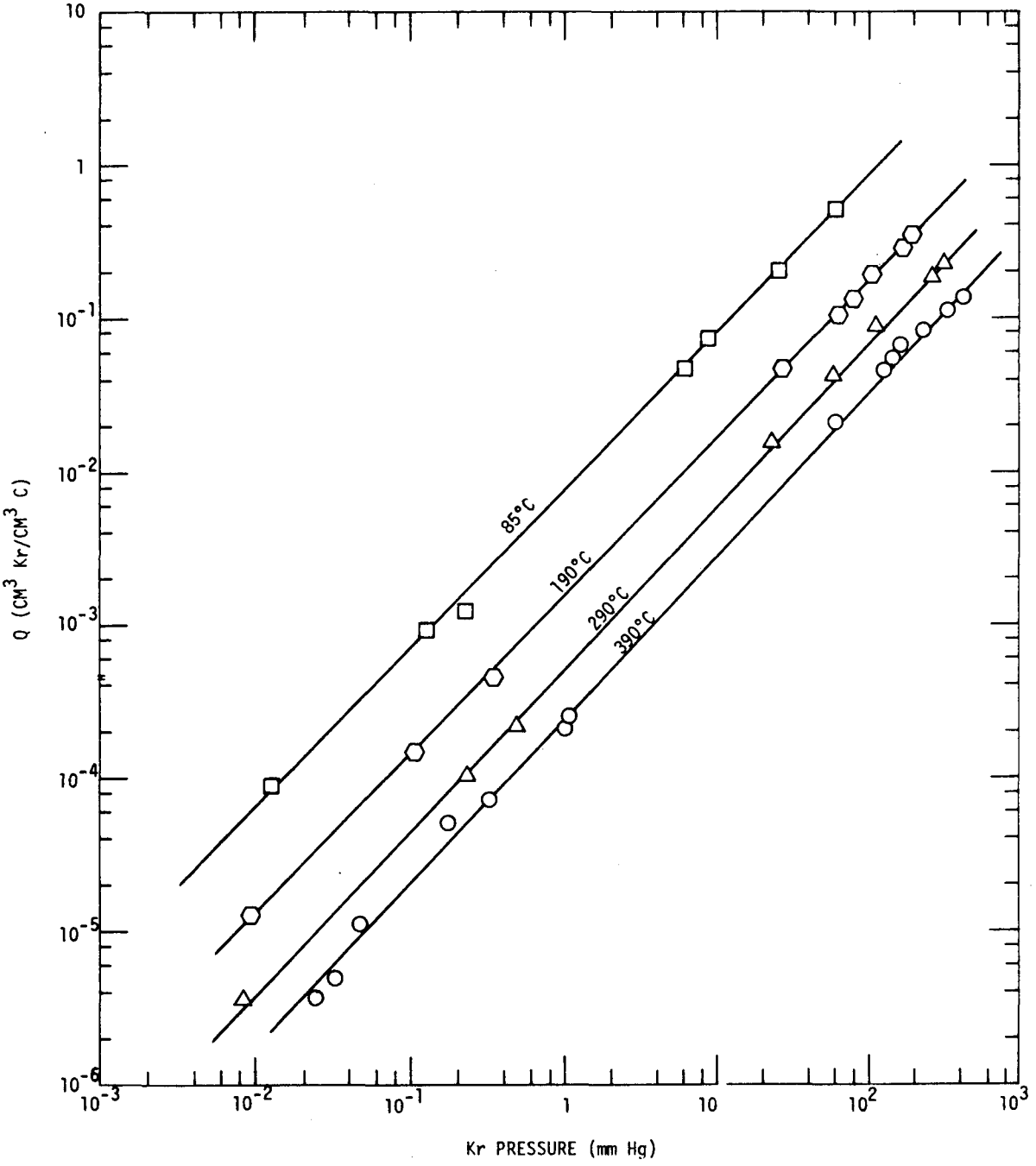

Fig. 4.9. Isotherms for krypton on carbon

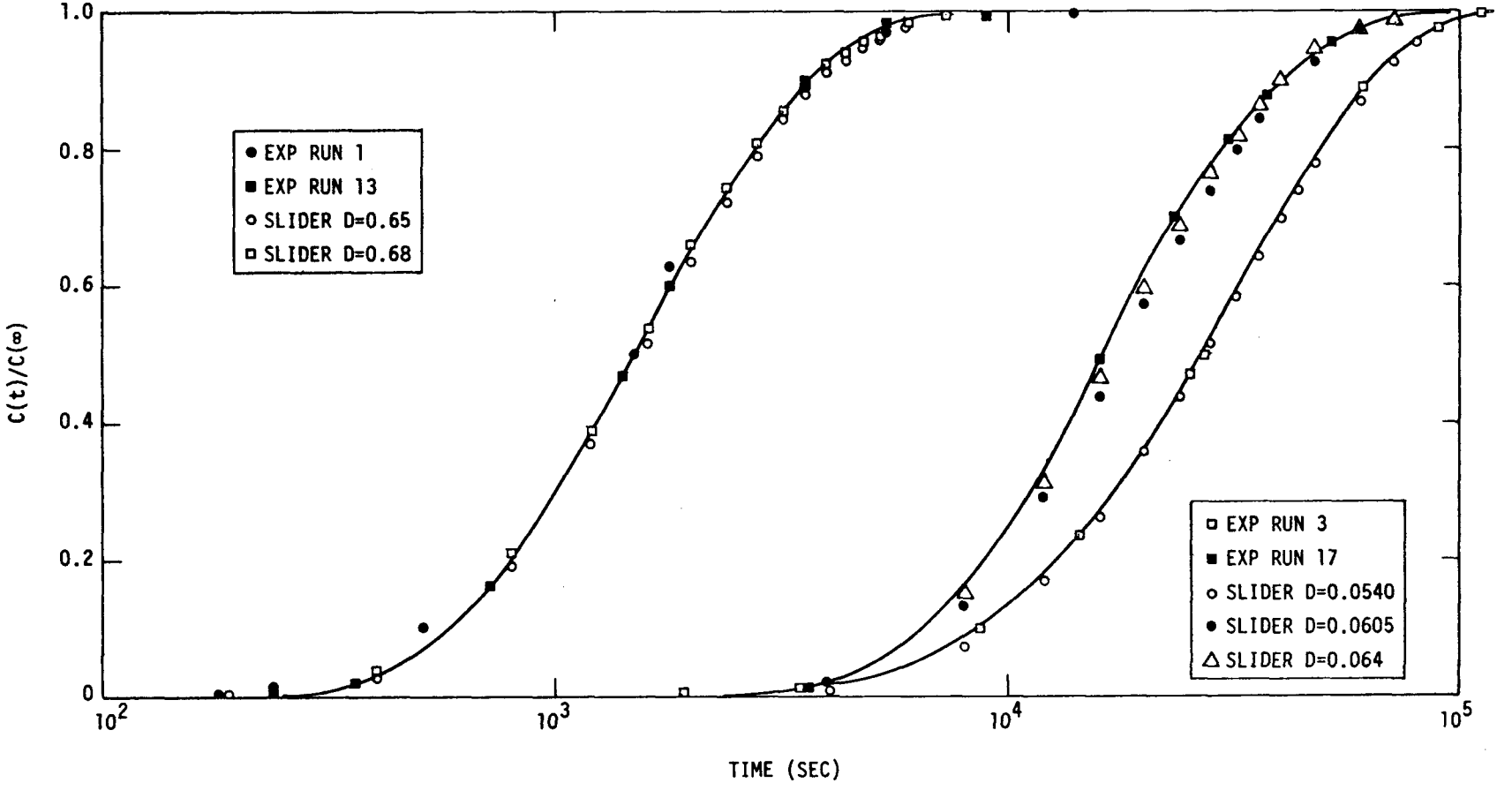

Fig. 4.10. Comparison of experimental krypton diffusion data with SLIDER analytical data

This expression was solved by hand computation for one typical set of conditions with the time selected to be near $C(t)/C(\infty) = 0.5$. Data from the corresponding SLIDER results were plotted, and a value of $C(t)/C(\infty) = 0.53 \pm 0.02$ was found at the corresponding time point. Comparison with the hand-computed series solution of the analytical expression (0.54257) shows satisfactory agreement.

The ion chamber which measures the arrival of krypton at the end of the diffusion tube is a cylinder of much greater diameter than the diffusion tube itself. Since SLIDER is only a one-dimensional program, some consideration was given to how to represent the chamber in the machine computations. In the experiments, the ion current generated results from ionization throughout the chamber. In other words, the ion chamber measures the total activity which enters the chamber. The resulting data are the currents proportional to the total activity in the chamber, and the ratio of these current values to the saturation value is determined. Thus, in the SLIDER representation it was possible to represent the ion chamber by a diffusion-tube length equivalent in volume to the ion chamber. The concentration of krypton in the chamber was then integrated and compared with a similar value computed after saturation was reached. Some small error results from this procedure, since the rate of activity entering the chamber depends on the downstream geometry as well as the volume. However, since the mean free path between collisions is several orders of magnitude smaller than the tube dimensions, wall effects are small.

Recent experiments of the same type which were performed by Bolch et al. (Ref. 2) at 1 atm have shown the diffusion coefficient of krypton in helium to be ∿10% smaller than that given by the standard equation. It has been reported (Ref. 2) that compilations of the data of other experimenters (Ref. 3) who used helium as one of the diffusion-couple members show coefficients that are consistently lower than those obtained from the equation. However, experiments performed in this laboratory at 1 atm yield values which agree closely with those calculated from the equation. Attempts are being made to resolve the difference between the values, including a review of instrumentation and geometry of the apparatus. For example, the ion chamber has a volume equivalent to 30.8 cm and a source length of 15 cm. In the measurements of Bolch et al., diffusion tubes 1 in. in diameter by 2 ft (∿60 cm) and 4 ft (∿120 cm) in length and 2 in. in diameter by 8 ft (∿240 cm) in length were used with a plane source, so the source and measuring instrumentation volumes were insignificant.

Runs 13, 14, 15, 16, and 17 were analyzed in addition to runs 1 and 3 to show the effect of pressure on the diffusion coefficient. An inverse pressure proportionality, such as that shown by the standard equation, was expected. The results (presented in Fig. 4.11 and Table 4.5) show that the inverse pressure relationship holds up to about 15 atm. Above 15 atm, the diffusion coefficient deviates significantly from the inverse relationship. A literature investigation will be made to determine the test range and limits of the inverse pressure relationship. Also, the ion chamber response at various pressures and concentrations will be reviewed to ensure that pressure and concentration are not factors contributing to a spurious non-proportionality to the inverse pressure.

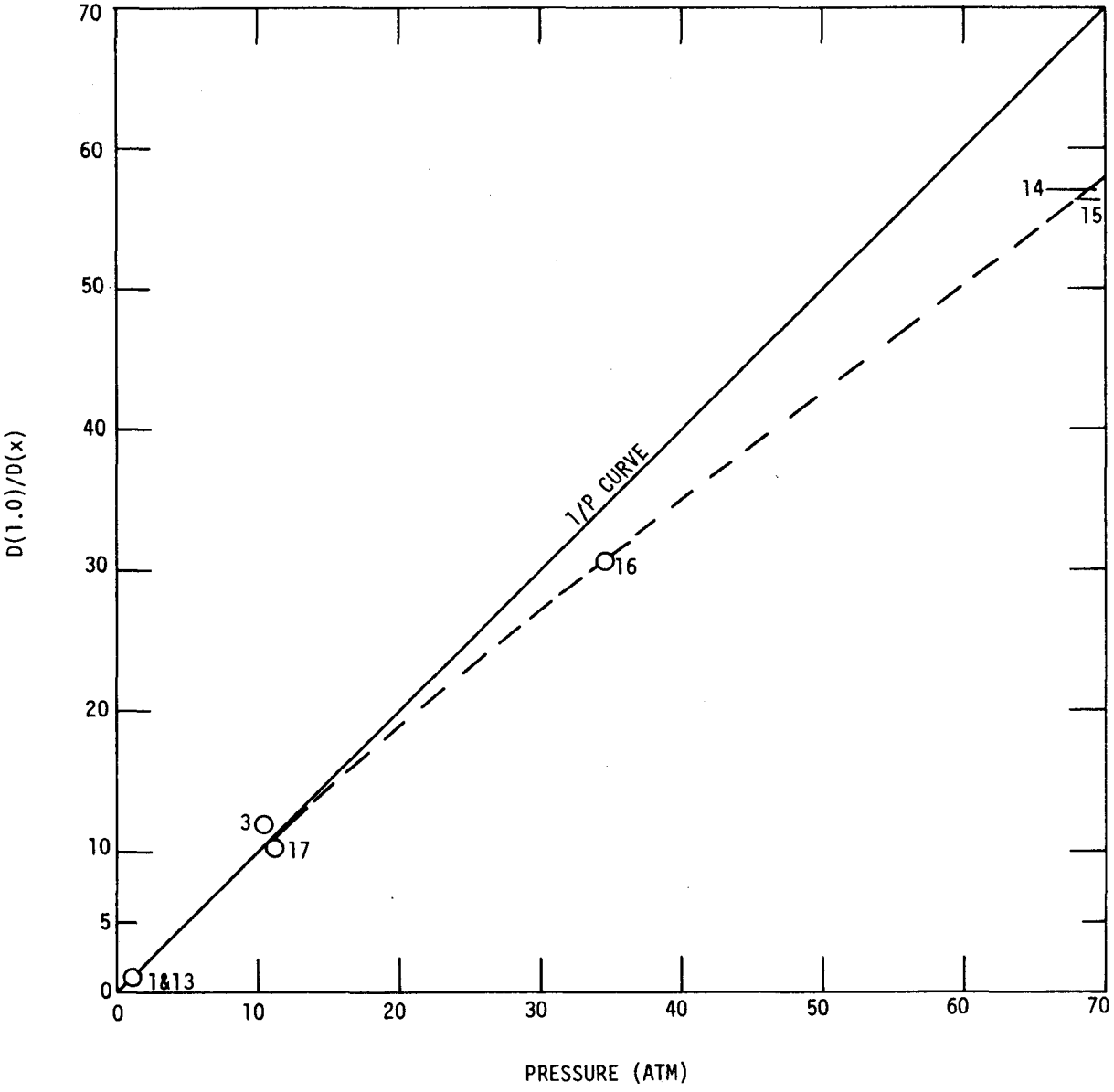

Fig. 4.11. Results of SLIDER analysis showing effect of pressure on diffusion coefficient

The experiments in which diffusion through blanket, fuel, and trap regions were simulated will be analyzed during the next reporting period.

Table 4.5

GASEOUS DIFFUSION COEFFICIENTS OF KRYPTON IN HELIUM

Run No.	Pressure (atm)	Diffusion Coefficients (cm^2/sec)
1	1.0	0.665
13	1.0	0.665
3	10.5	0.0549
17	11.0-11.2	0.0652
16	34.7-34.8	0.0216
14	66.0-69.5	0.0116
15	68.1-69.5	0.0118

4.3.2. Fast-Flux Capsule Irradiations

The design of the fast-flux irradiation capsules for EBR-II is continuing. An EBR-II experimenters meeting was attended at Idaho Falls, where discussions were held with ANL EBR-II project personnel. As a result of these discussions, it is proposed to use one of the standard subassemblies with the minimum modification to meet the GCFR requirements.

Typical test conditions for the initial subassembly are:

Cladding OD surface temperature	650°-750°C
Cladding	316 SS
Cladding OD	0.250-0.350 in.
OD/ID	∿1.15
Linear power generation (max)	∿15 kW/ft
Fuel	85 UO_2-15 PuO_2
Fuel smear density	≤85% TD
External pressure	Ambient
Bond-gap fluid	Helium
Initial internal pressure, hot	40 psig
End-of-life internal pressure, hot	<250 psig
Burnup goal	>50,000 MWD/tonne (15 x 10^{20} f/cm^3)

The general objective of the fast-flux tests is to test fuel-rod specimens under those combinations of conditions which differentiate the GCFR fuel rod from the LMFBR fuel pin, with particular attention to the higher range of cladding temperatures not presently included in the LMFBR test program. The specific test objectives for capsules in the initial EBR-II subassembly are:

1. To determine the integral irradiation behavior of 316-stainless-steel-clad plutonium-uranium oxide fuel rods which simulate a manifolded rod at nominal GCFR conditions, i.e., a maximum cladding temperature of 700°C, heat generation rates of ∿15 kW/ft (max), and an average burnup of ∿50,000 MWD/tonne. These conditions are expected to be in the range where irradiation embrittlement of the cladding and fuel swelling are significant.

2. To determine the effect of irradiation on fuel-rod behavior with cladding surface temperatures in the range from 650° to 750°C under typical combinations of GCFR operating conditions.

3. To observe the effect of providing a fission-product trap (exposed to fast-flux damage) on the fission gas released by the $(Pu,U)O_2$-fueled rod.

4. To provide a comparison between the behavior of fuel rods operating in a fast flux with a pressure equalization (or low pressure differential) and that of a similar fuel rod (GA-20) which will be irradiated in an instrumented thermal flux (P9).

5. To provide a comparison between the behavior of manifolded fuel rods and that of sealed-can, fuel-cladding-interacting fuel rods after high burnup; specifically, to compare the behavior of the manifolded rods with the behavior of sealed-can, fuel-cladding-interacting rods GA-17, -18, and -19 that were irradiated in capsule P8 to similar burnups.

6. To determine the effect of irradiation on the mechanical, physical, and chemical properties and behavior of the fuel and cladding. Specific effects include changes in ductility and void formation in cladding, fuel microstructural changes, and fuel-cladding mechanical and chemical interactions. Evaluation of these effects will require comparison with prior results from GCFR irradiations and with the extensive results from the LMFBR test program.

7. To determine the combined effect of fast-flux irradiation and GCFR operating temperature on the candidate GCFR cladding and structural materials in separate nonfueled capsules within the subassembly. These nonfueled-capsule tests would include indicators (other than instrumentation) that would allow temperature effects to be determined and to be correlated with the effects observed in the fuel-rod capsules.

The most important aspect of the capsule design is the achievement of cladding temperatures in the range from 650° to 750°C. Most of the fast-flux irradiations conducted to date have been for cladding temperatures of ∿550°C in EBR-II. Assemblies with cladding temperature approaching 650°C have been prepared for the LMFBR program, and their irradiation in EBR-II will begin in the near future. Therefore, the GCFR program will be concentrated on the maximum temperature of interest to early demonstration cores (∿700°C) and higher temperatures. Three design approaches appear capable of achieving the GCFR objectives.

The initial study has been on the use of a standard 19-pin assembly in which a gas-gap type of thermal barrier is employed to increase the cladding temperatures. It is anticipated that an experimental program might be required to reduce calculational uncertainties. The details of this design are shown in Fig. 4.12. The subassembly design would be identical to those now operational in EBR-II and uses a standard 19-pin subassembly (type A-19 or B-19).

Another approach would be to use the type J-19 subassembly, which has a circumferential insulated flow bypass, to increase the sodium temperatures in the inner test section prior to mixing and exiting from the EBR-II core. A preliminary analysis has been initiated on the cladding temperatures which could be obtained. The first operation of this subassembly for the LMFBR program at cladding temperatures approaching 650°C is expected to take place this year.

It appears that the type B-7 subassembly is capable of meeting all the thermal and size requirements for the GCFR test program. Preliminary calculations indicate that sufficient space would be available within the capsule to allow the use of conventional thermal barriers similar to those used in thermal-flux capsules to obtain the desired cladding temperatures. Since the B-7 subassembly has been used for testing structural materials, some modification of the standard B-7 subassembly would be required for fuel testing. The necessary changes would probably include use of shroud tubes around the capsules, as in the A-19 subassembly.

4.3.3. ATR Gas Loop

Late in the reporting period, information was received from Pacific Northwest Laboratory representatives at NRTS briefly describing the Gas-Cooled Loop Systems and Components (GCL) in the ATR and some preliminary considerations regarding the loop's applicability to the GCFR fuel-element irradiation program. This information will be evaluated, and any significant results will be presented in subsequent reports.

4.4. THERMAL-CYCLING RIG

The capabilities of the thermal-cycling rig are being checked out at higher power levels. The improved test chambers have been assembled and are in use. The transverse section of the assembly, which operated for 245 hr at 5.5 kW/ft with cladding temperatures up to 790°C, was examined

in the electron microprobe for cladding-UO_2 reactions. The results are given in Ref. 1. No evidence of diffusion of any of the components was noted, and the chromium concentration was not depleted near the interface. Small amounts of iron and chromium were found on the edge of the UO_2 but not in any of the radial cracks. Nickel and molybdenum were found only in the cladding and were uniformly distributed.

A sample which was set up for testing at 8 kW/ft proved unsuccessful due to thermocouple attachment problems which caused a wide variation in the indicated temperature (150° to 600°C). The spot-welding procedures for thermocouple attachment were then improved, and the next run attempted at 8 kW/ft was successful. The test was conducted for 258.1 hr with cladding temperatures from 780° to 880°C at 8.3 kW/ft and from 710° to 900°C at 7.05 kW/ft near the end of the run. The drop in power was caused by vaporization loss of tungsten from the center of the heater, which required more voltage. However, the controller was operating near the limiter settings, so sufficient additional power was not available. Voltage tap changes on the output transformer were made and a 10 kW/ft run was conducted for 103.4 hr with cladding temperatures of 602° to 625°C.

After this run the heater rod was in good shape, with a slightly decreased diameter. A transverse metallographic sample taken from near the midlength of the heated zone was examined (see Fig. 4.13). The UO_2 fuel was cracked, and its appearance indicated that it had experienced a very high temperature near the surface of the central hole near the tungsten heater. Extensive grain growth typical of UO_2 operation above 1800°C had occurred in this region, resulting in a structure consisting of a mixture of large equiaxed and columnar grains. Some grain growth, though rapidly decreasing in extent, was observed to the midradius of the fuel (indicating that the UO_2 had operated at $\sim$1500° to 1600°C at midradius). The outer portions of the UO_2 showed little if any change in structure except for cracking (primarily radial in direction). Tungsten from the heater had penetrated the grain boundaries, pores, and cracks in the UO_2 to a depth of $\sim$20 mils from the surface of the central hole. It is not clear whether the tungsten penetration resulted from diffusion or vapor deposition, or both; but the tungsten penetration ends abruptly (though at different depths) on all sides of the pellet in the section examined. A test to run at 12 kW/ft was unsuccessful due to burnout after 4 hr at 11.5 kW/ft and cladding temperatures of 700° to 820°C.

The purpose of this phase of the checkout procedures is to make steady-state runs of 100 to 250 hr. However, during each run to date there has been at least one automatic shutdown due to either high cladding temperature or limit switches being tripped as a result of high or low helium gas flow. These shutdowns have usually occurred at night or over the weekend, resulting in test-sample cooldown to room temperature. No difficulty has been experienced in restarting tests from room temperature, indicating that the cyclic testing should be able to operate over a wide temperature range. Two more steady-state runs at 12 and 14 kW/ft are planned before the start of cyclic testing.

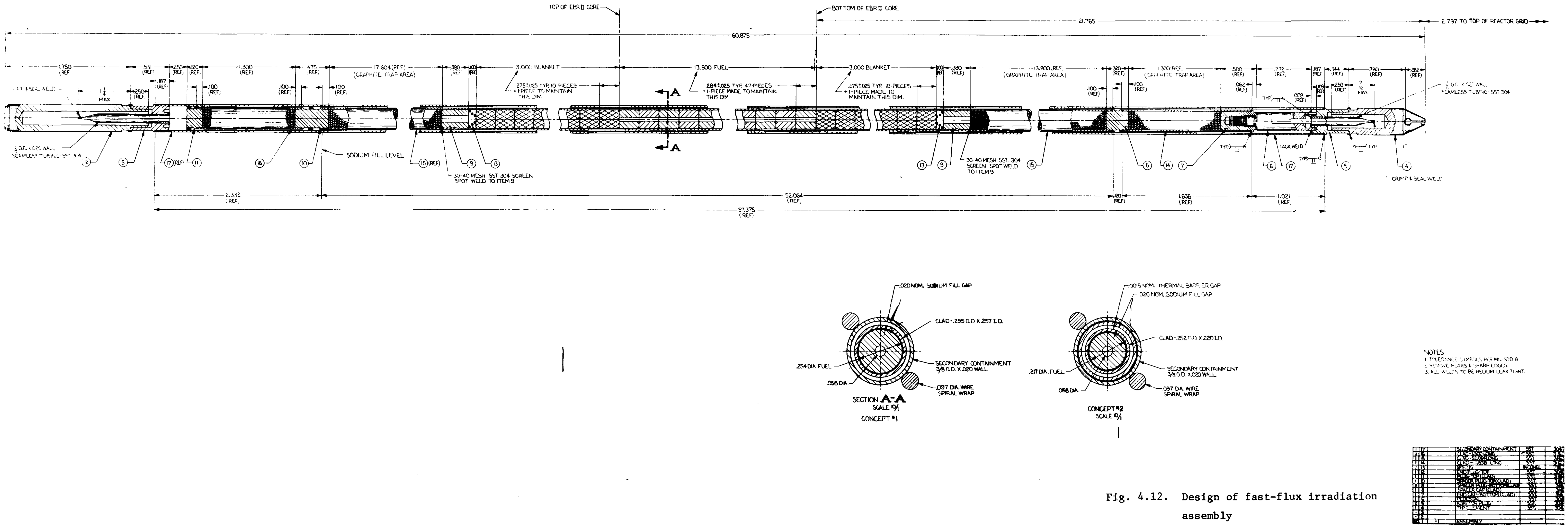

Fig. 4.12. Design of fast-flux irradiation assembly

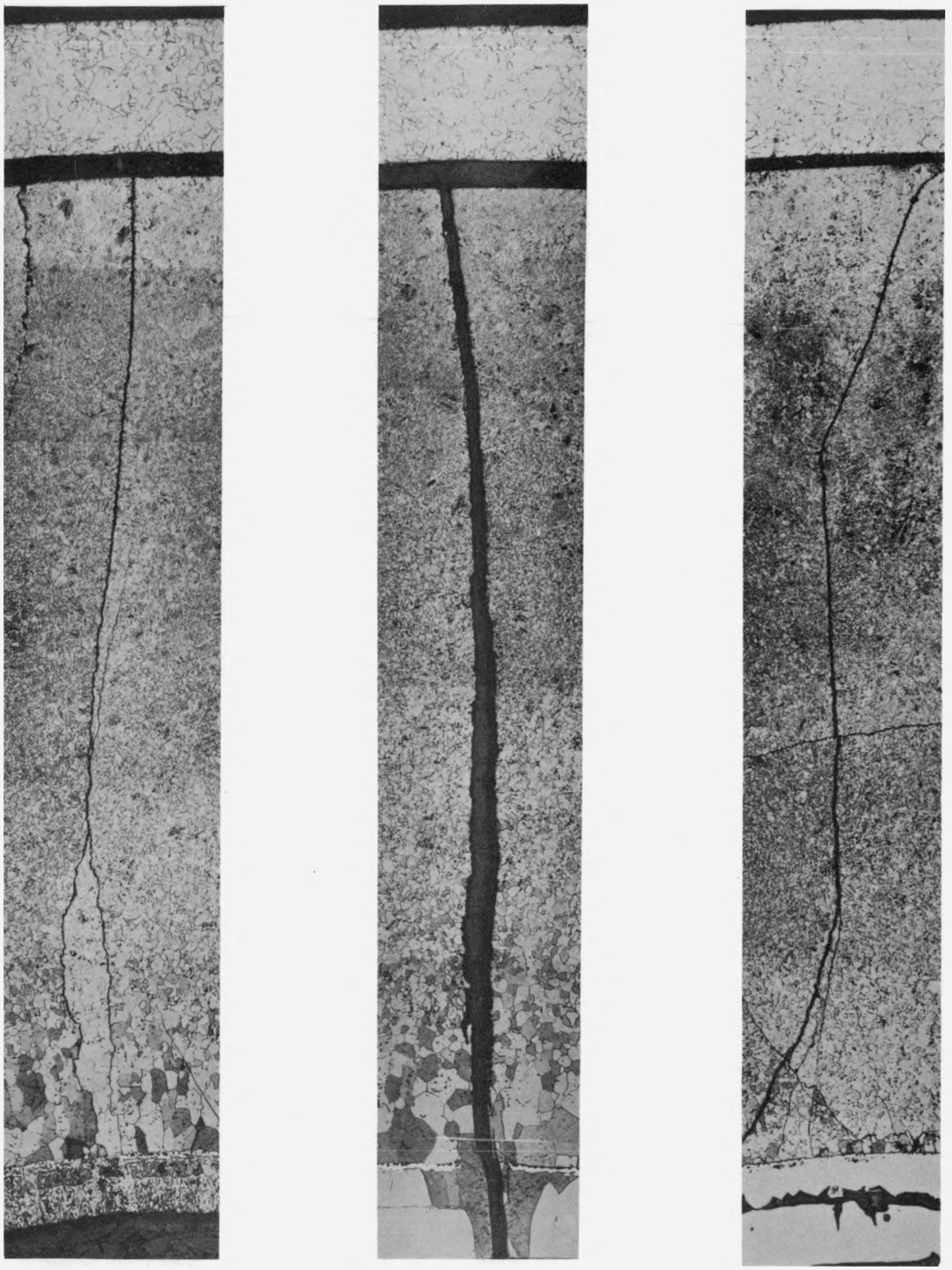

M29822

Fig. 4.13. Transverse metallographic sample showing results of 10 kW/ft thermal-cycling run after 103.4 hr

REFERENCES

1. "Gas-Cooled Fast Breeder Reactor. Quarterly Progress Report for the Period November 1, 1968 through January 31, 1969," USAEC Report GA-9229, Gulf General Atomic Incorporated, March 24, 1969.

2. Bolch, W. Emmett, Robert E. Selleck, and Warren J. Kaufman, "Gas Dispersion in Porous Media Pedet-Reynolds Number Correlations," USAEC Report SERL No. 67-10, University of California, Berkeley, Sanitary Engineering Research Laboratory, 1967.

3. Reid, R. C., and T. K. Sherwood, Properties of Gases and Liquids, McGraw-Hill Book Company, New York, 1966.

5. TASK D - REACTOR PHYSICS PROGRAM

During the latter half of April, permission was received from the Battelle-Northwest criticality review committee to proceed with the 1/1 H/Pu critical experiments, and the planned program has been started.

To date, critical size and height measurements have been made of a bare, unpoisoned assembly and an assembly containing dysprosium oxide. The aim of these initial experiments is to determine a suitable "base case" and to evaluate required experimental corrections, such as temperature and coating-thickness corrections, and reproducibility.

As was anticipated from the initial critical-mass calculations, the amount of plutonium fuel available in the 1/1 H/Pu ratio is not sufficient to construct a bare, critical assembly. Therefore, fuel with a 5/1 H/Pu ratio is being used as a driver region in these assemblies to achieve criticality. This is not expected to cause any major difficulties in the analysis of the 1/1 H/Pu ratio assemblies, since the results of the analysis of the previous 5/1 H/Pu critical experiment program (Ref. 1) revealed good agreement between theory and experiment.

REFERENCE

1. "Gas-Cooled Fast Breeder Reactor. Annual Progress Report for the Period Ending July 31, 1967," USAEC Report GA-8107, Gulf General Atomic Incorporated, 1968, Section 5.